iScience

CellPress
OPEN ACCESS

Article

Epigenetic modifier SMCHD1 maintains a normal pool of long-term hematopoietic stem cells

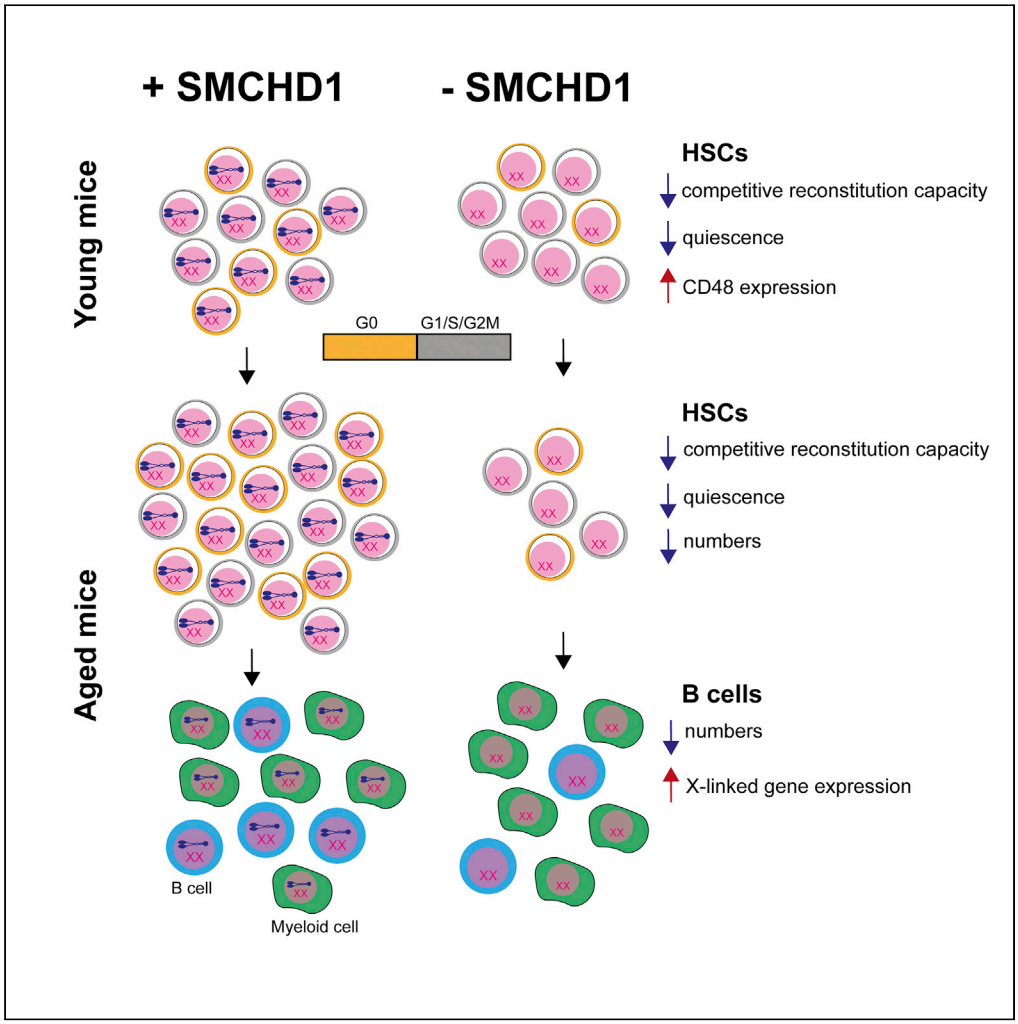

Sarah A. Kinkel, Joy Liu, Tamara Beck, Kelsey A. Breslin, Megan Iminitoff, Peter Hickey, Marnie E. Blewitt

blewitt@wehi.edu.au

Highlights

SMCHD1 is not required to maintain steady-state hematopoiesis

Smchd1-deletion leads to loss of adult hematopoietic stem cells

Smchd1-deleted female mice are more severely affected than males

SMCHD1 maintains cellular quiescence in female hematopoietic stem cells

Kinkel et al., iScience *25*, 104684
July 15, 2022
https://doi.org/10.1016/j.isci.2022.104684

iScience

CellPress
OPEN ACCESS

Article

Epigenetic modifier SMCHD1 maintains a normal pool of long-term hematopoietic stem cells

Sarah A. Kinkel,[1,2] Joy Liu,[1,2] Tamara Beck,[1] Kelsey A. Breslin,[1] Megan Iminitoff,[1,2] Peter Hickey,[1,2] and Marnie E. Blewitt[1,2,3,*]

SUMMARY

SMCHD1 (structural maintenance of chromosomes hinge domain containing 1) is a noncanonical SMC protein that mediates long-range repressive chromatin structures. SMCHD1 is required for X chromosome inactivation in female cells and repression of imprinted and clustered autosomal genes, with *SMCHD1* mutations linked to human diseases facioscapulohumeral muscular dystrophy (FSHD) and bosma arhinia and micropthalmia syndrome (BAMS). We used a conditional mouse model to investigate SMCHD1 in hematopoiesis. *Smchd1*-deleted mice maintained steady-state hematopoiesis despite showing an impaired reconstitution capacity in competitive bone marrow transplantations and age-related hematopoietic stem cell (HSC) loss. This phenotype was more pronounced in *Smchd1*-deleted females, which showed a loss of quiescent HSCs and fewer B cells. Gene expression profiling of *Smchd1*-deficient HSCs and B cells revealed known and cell-type-specific SMCHD1-sensitive genes and significant disruption to X-linked gene expression in female cells. These data show SMCHD1 is a regulator of HSCs whose effects are more profound in females.

INTRODUCTION

SMCHD1 (Structural maintenance of chromosomes hinge domain containing 1) is a noncanonical SMC protein first identified as an epigenetic repressor in a screen for epigenetic modifiers of transgene variegation performed in mice (Blewitt et al., 2005). SMCHD1 has since been shown to play a critical role in both random X chromosome inactivation (XCI) in female embryos, and imprinted XCI in the placenta, with *Smchd1*-null females failing to survive past mid-gestation (Blewitt et al., 2005, 2008; Gendrel et al., 2012). In male mice, *Smchd1*-deficiency can also lead to perinatal lethality dependent on genetic background (Blewitt et al., 2008; Leong et al., 2013; Mould et al., 2013). SMCHD1 has moreover been shown to repress a subset of clustered autosomal genes, with a role in maintaining monoallelic expression of some imprinted genes, such as those within the Prader-Willi Syndrome/*Snrpn* cluster, and silencing the clustered protocadherins and *Hox* genes (Chen et al., 2015; Gendrel et al., 2013; Jansz et al., 2018; Mould et al., 2013; Wanigasuriya et al., 2020).

SMCHD1 function is highly relevant to human disease, with heterozygous *SMCHD1* mutations found in two separate disorders: FSHD and BAMS (Gordon et al., 2017; Jansz et al., 2017; Lemmers et al., 2012; Shaw et al., 2017). In FSHD, heterozygous loss-of-function mutation of *SMCHD1* results in relaxation of repressive chromatin structures at the *D4Z4* macrosatellite repeat, leading to aberrant, variegated expression of the myotoxic gene *DUX4* in skeletal muscle (Jansz et al., 2017; Lemmers et al., 2012). In BAMS, pathogenic *SMCHD1* missense mutations fall exclusively within its extended ATPase domain; however, reports differ as to whether these variants lead to a loss or gain of SMCHD1 function (Gordon et al., 2017; Gurzau et al., 2018; Jansz et al., 2017; Lemmers et al., 2019; Shaw et al., 2017).

Mechanistically, SMCHD1 works by maintaining long-range repressive chromatin structures; in the case of the inactive X chromosome (Xi), ablation of SMCHD1 leads to a strengthening of short-range interactions, altering the Xi architecture such that it adopts a structure more reminiscent of its active counterpart (Gdula et al., 2019; Jansz et al., 2018; Wang et al., 2018). Studies using mouse embryonic fibroblasts and primary neural stem cells suggest a role for SMCHD1 in insulating chromatin by limiting promoter-enhancer interactions and access to other epigenetic modifiers both

[1]The Walter and Eliza Hall Institute of Medical Research, 1G Royal Parade, Parkville, VIC 3052, Australia

[2]The Department of Medical Biology, The University of Melbourne, Parkville, VIC 3010, Australia

[3]Lead contact

*Correspondence: blewitt@wehi.edu.au

https://doi.org/10.1016/j.isci.2022.104684

at the Xi and autosomal gene targets (Chen et al., 2015; Gdula et al., 2019; Jansz et al., 2018; Wang et al., 2018).

SMCHD1's involvement in several human diseases marks it as an attractive potential therapeutic target and makes it important to understand how altering its function may affect different biological systems. Here we sought to investigate the role SMCHD1 plays in blood cell development, given the exposure of this system to almost any drug intervention. HSCs with long-term self-renewal and differentiation capacity generate the myriad of highly specialized blood cells types required for the duration of an animal's lifetime, with perturbation to HSC function resulting in altered cellular output, increased incidence of hematopoietic malignancies, and a reduced ability to fight infection (Eaves, 2015; Haas et al., 2018; Orkin and Zon, 2008).

Whereas no obvious hematological phenotype has been reported in FSHD and BAMS patients harboring heterozygous *SMCHD1* mutations, several studies prompted us to suspect a role for SMCHD1 in blood cells. DNA methylation analysis of FSHD patient-derived mononuclear cells showed hypomethylation at known autosomal target gene clusters (Mason et al., 2017), and previous work from our lab has shown that *Smchd1*-deletion in male fetal liver cells accelerates the development of Eμ-Myc transgene-driven B cell lymphoma (Leong et al., 2013). In zebrafish, *smchd1* was recently identified as a signature gene in hematopoietic stem and progenitor cells (HSPCs) that is required for their expansion during development, with *smchd1*-depletion resulting in reduced HSPC numbers (Xue et al., 2019). Furthermore, deletion of *Xist*, the long non-coding RNA required for X chromosome inactivation, results in an aggressive myeloproliferative neoplasm in female mice and proposes that proper maintenance of X inactivation is required to prevent aberrant hematopoiesis (Yildirim et al., 2013); suggesting that as an X inactivation regulator, SMCHD1 may also be required for hematopoiesis.

Here we analyzed mice with a blood-specific deletion of *Smchd1* and found that SMCHD1 plays a role in both male and female HSCs. Whereas we observed minimal disruption to steady-state hematopoiesis, *Smchd1*-deleted bone marrow showed reduced repopulation capacity in competitive transplantation assays and a loss of classically defined HSCs in aged animals. This phenotype was more pronounced in *Smchd1*-deleted females, which showed an altered cell surface staining profile within the HSPC compartment and a reduced proportion of quiescent HSCs in the G_0 stage of the cell cycle, as well as a lack of the normal age-related expansion of long-term HSCs. There was also a significant decrease in the number of B lymphocytes in the bone marrow of aged *Smchd1*-deleted females. Gene expression profiling of hematopoietic cells lacking *Smchd1* revealed cell-type-specific SMCHD1-sensitive genes, whereas several known autosomal SMCHD1 targets were upregulated in *Smchd1*-deleted B cells. Whereas there was no easily detectable widespread upregulation of X-linked transcripts in *Smchd1*-deleted female HSCs, X-linked genes were more commonly disrupted in their expression than in controls. These data confirm SMCHD1 as a regulator of adult HSC maintenance with a more striking role in females and suggest SMCHD1 may be required to protect the epigenetic state of the inactive X chromosome in these cells.

RESULTS

SMCHD1 is expressed in HSPCs

Whereas SMCHD1 plays a critical role in X chromosome inactivation in female cells, it has a ubiquitous expression pattern in both female and male cells and also regulates autosomal gene expression in several different cell types (Blewitt et al., 2005, 2008; Chen et al., 2015; Gendrel et al., 2013; Jansz et al., 2018; Mould et al., 2013).

Interrogation of publicly available expression data sets shows that *Smchd1* mRNA is expressed throughout the hematopoietic system (Figure S1A) (Bagger et al., 2019). To further examine SMCHD1 expression, we used $Smchd1^{GFP}$ knock-in mice (Jansz et al., 2018) that express a functional SMCHD1-GFP fusion protein detectable by flow cytometry. Analysis of bone marrow from young and aged $Smchd1^{GFP/GFP}$ mice confirmed SMCHD1-GFP expression in lineage$^-$ c-kit$^+$ Sca1$^+$ CD48$^-$ CD150$^+$ long term (LT)-HSCs (Figure 1A), as well as in both B lymphocytes and myeloid cells (Figure S1B), with a shift in the entire cell population to being GFP$^+$ compared with $Smchd1^{+/+}$ controls. Of the cell populations examined, B cells appeared to have the highest level of *Smchd1*/SMCHD1 expression (Figures 1A, S1A, and S1B). We observed no significant differences in SMCHD1-GFP mean fluorescence intensity (MFI) between males and females in any of the cell types analyzed (Figures 1A and S1B); however, we did observe a small but significant reduction in Smchd1-GFP MFI in aged female myeloid cells (Figure S1B), perhaps indicative of a reduced requirement for SMCHD1 in this cell type with age.

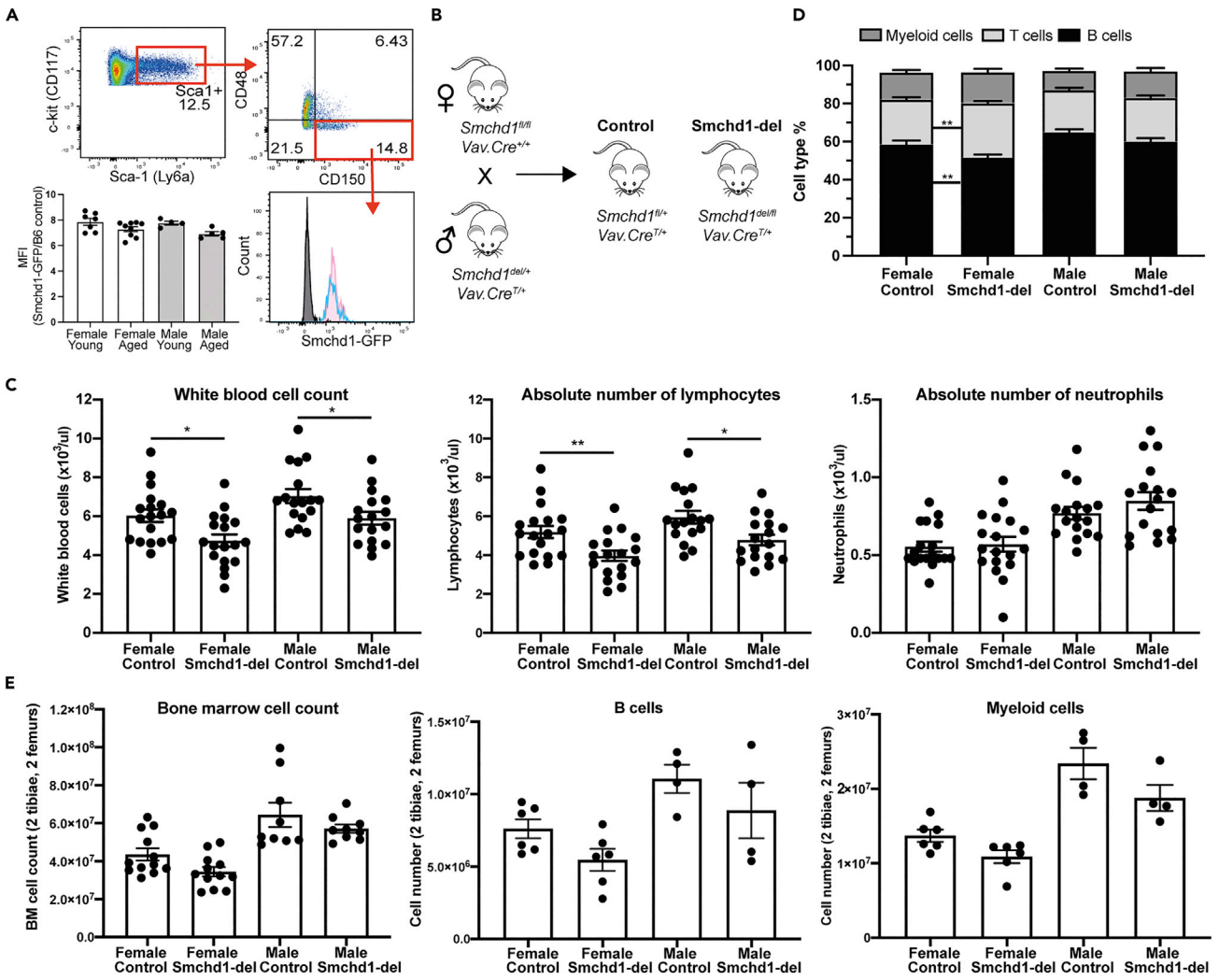

Figure 1. *Smchd1* deletion leads to minimal changes to steady-state hematopoiesis in mice

(A) Smchd1-GFP is expressed in long-term hematopoietic stem cells (LT-HSCs). Representative flow cytometry plots showing Sca1$^+$ HSPCs (gated on lineage$^-$ c-kit$^+$ cells) that are further divided into MPP and HSC subsets by CD48 and CD150 staining. Histogram shows Smchd1-GFP expression in LSK CD48$^-$ CD150$^+$ LT-HSCs (bottom) for C57BL/6 (black), Smchd1-GFP female (pink), and Smchd1-GFP male (blue). Plots are representative of three separate experiments. The graph shows the mean fluorescence intensity for Smchd1-GFP compared with C57BL/6 controls in LT-HSCs.

(B) Breeding strategy for generating mice with a blood-specific deletion of *Smchd1*.

(C) White blood cell and lymphocyte, but not neutrophil numbers are reduced in the peripheral blood of Smchd1-del mice.

(D) Proportions of B220$^+$ B cells, CD4$^+$/CD8$^+$ T cells, and Mac1$^+$/CD11b$^+$ myeloid cells gated on CD45.2$^+$ cells in the peripheral blood are shown for Smchd1-del animals and controls, indicating altered lymphocyte proportions in Smchd1-del females.

(E) Total BM cell numbers, B cell, and myeloid cell numbers are not significantly different between Smchd1-del mice and controls. Data were statistically analyzed by one-way ANOVA with Sidak multiple comparisons test comparing control with Smchd1-del for each sex using Prism 9. *$p < 0.05$, **$p < 0.01$, ***$p < 0.001$. All error bars for the figure represent SEM.

SMCHD1 is essential for the viability of female mouse embryos (Blewitt et al., 2008), thus, to investigate whether SMCHD1 plays a role in hematopoiesis, we generated mice with a blood cell lineage-specific deletion of *Smchd1* by crossing *Smchd1*$^{fl/fl}$ mice (de Greef et al., 2018) to *Smchd1*$^{del/+}$ mice carrying a *Vav.Cre* transgene (Croker et al., 2004) (Figure 1B). We kept the *Vav.Cre* transgene with the *Smchd1* deleted and wild-type alleles for breeding because *Vav.Cre* is known to have some expression in the germline (Croker et al., 2004; Ogilvy et al., 1999). This breeding strategy generated *Vav.Cre* transgenic mice that were *Smchd1*-deleted (*Smchd1*$^{del/fl}$ *Vav.Cre*$^{T/+}$; Smchd1-del) or *Smchd1* heterozygous (*Smchd1*$^{fl/+}$ *Vav.Cre*$^{T/+}$; Control) within the blood cell lineage. These heterozygous littermates were used as controls for all experiments as heterozygous loss of *Smchd1* has no phenotypic effect on the hematopoietic system (Leong et al., 2013).

RT-qPCR performed on lineage$^-$ c-kit$^+$ bone marrow cells from control (*Smchd1*$^{fl/+}$ *Vav.Cre*$^{T/+}$) and Smchd1-del (*Smchd1*$^{del/fl}$ *Vav.Cre*$^{T/+}$) animals confirmed that expression of *Smchd1* mRNA is significantly reduced in Smchd1-del hematopoietic cells (Figure S1C). Previous analysis of *Smchd1*-deleted cells derived from the *Smchd1*$^{fl/fl}$ mouse line reveals that whereas low levels of *Smchd1* mRNA are detectable post deletion, there is no detectable SMCHD1 protein (Jansz et al., 2018).

Within the colony, fewer female Smchd1-del mice were observed than expected at weaning (Figure S1D). Based on the cross we expect one-quarter of the females to be *Smchd1*$^{del/fl}$ *Vav.Cre*$^{T/+}$, yet only 15 of the 142 female mice to reach weaning age had this genotype (Chi-squared test $p = 0.0002$). By contrast, the expected 41 of the 167 male mice carried the *Smchd1*$^{del/fl}$ *Vav.Cre*$^{T/+}$ genotype.

Those Smchd1-del females present in adulthood weighed less (control: 29.6 $\pm$ 3.4g; Smchd1-del: 24.5 $\pm$ 3.4g) than age-matched cage mate or littermate controls (*Smchd1*$^{fl/+}$ *Vav.Cre*$^{T/+}$), whereas no difference in weight was observed between male mice of differing genotypes (Figure S1E). The Smchd1-del adult females that were present appeared otherwise healthy, with mice monitored beyond 12 months of age showing no increased incidence of illness. Given these sex-specific differences and the known female-specific role of SMCHD1 (Blewitt et al., 2008), animals were separated by sex for all analyses.

SMCHD1 is required for normal white blood cell numbers in the peripheral blood

Analysis of peripheral blood from adult (four- to eight-month old) mice showed a reduction in white blood cell (WBCs) and lymphocyte numbers in both female and male Smchd1-del mice compared with controls, whereas neutrophil numbers were unchanged (Figure 1C). We observed no difference in red blood cell numbers, whereas platelet counts were slightly decreased in Smchd1-del mice (Figure S1F). Flow cytometry analysis indicated a skewing of lymphocyte proportions in the peripheral blood of female Smchd1-del mice, with a significant reduction in the proportion of B220$^+$ B cells and an increase in the proportion of CD4$^+$/CD8$^+$ T cells (Figure 1D).

Further analysis of hematopoietic organs showed that Smchd1-del mice have normal proportions of developing thymocytes (Figure S1G), lymphocytes, and myeloid cells in the spleen and bone marrow (Figure S1H). Furthermore, total cell number, B cell, and myeloid cell numbers in the bone marrow (BM) of Smchd1-del animals were not significantly different from controls (Figure 1E).

These data suggest that deletion of *Smchd1* in the blood system does not lead to any major disruptions in steady-state hematopoiesis in young, unmanipulated animals. Consistent with this, *Smchd1* null males, homozygous for the nonsense mutation *MommeD1* on an FVB/N genetic background, have normal peripheral blood cell counts (Figure S1I). Given the expression of SMCHD1 throughout the hematopoietic system and the potential deletion of *Smchd1* in some non-hematopoietic tissues owing to *Vav.Cre* leaky expression (Croker et al., 2004; Ogilvy et al., 1999), we sought to further investigate how *Smchd1* deletion may affect the behavior of HSCs by testing their reconstitution capacity. We chose to continue with the conditional deletion model as it affords the opportunity to also study female hematopoetic cells, which is not possible otherwise.

SMCHD1 is required to maintain bone marrow reconstitution potential

To test whether the loss of SMCHD1 affects bone marrow reconstitution capacity in a competitive setting, we transplanted 2×10^6 CD45.2$^+$ control or Smchd1-del whole BM cells into lethally irradiated CD45.1$^+$ recipients in competition with 2×10^5 CD45.1$^+$/CD45.2$^+$ whole BM cells (10:1 ratio, Figure 2A). Mice were analyzed for reconstitution of the peripheral blood with CD45.2$^+$ donor-derived cells at 6 and 12 weeks post-transplant with the contribution of donor cells to BM, spleen, and thymus analyzed at 20 weeks post-transplant, thereby allowing us to gauge both short- and long-term reconstitution potential.

At all time-points analyzed post-transplant, the ratio of CD45.2$^+$ test cells to CD45.1$^+$/CD45.2$^+$ competitor cells observed in recipients transplanted with control BM was equivalent to the input cell proportion (Figure 2B). As our control samples are heterozygous for the *Smchd1*^{del} allele in the blood, these data suggest that there is no loss of competitive fitness in BM cells heterozygous for *Smchd1* under these experimental conditions.

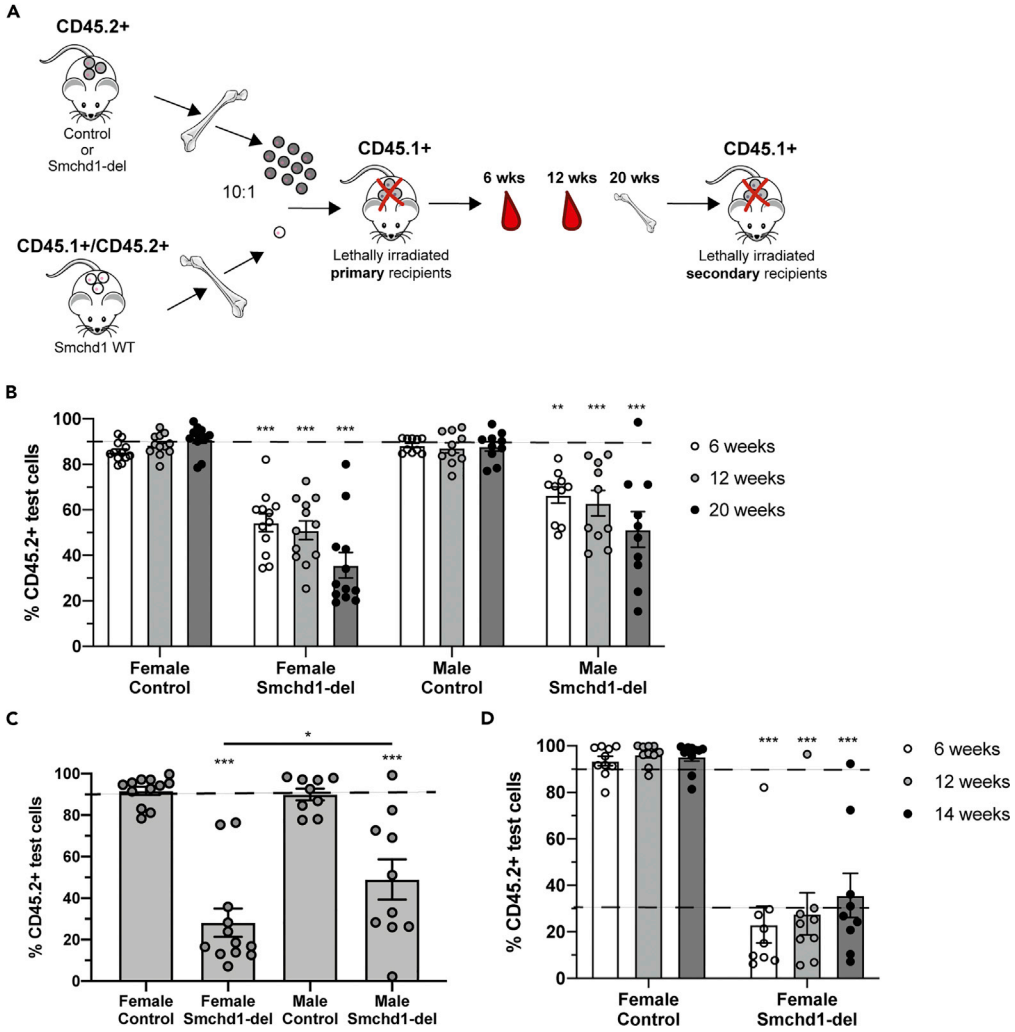

Figure 2. SMCHD1 is required for normal bone marrow reconstitution capacity in competitive bone marrow transplantation assays

(A) Competitive BMT assay: control or Smchd1-del CD45.2$^+$ whole BM cells were transplanted into lethally irradiated CD45.1$^+$ recipient mice in competition (10:1 ratio) with CD45.1$^+$/CD45.2$^+$ whole BM from 6- to 8-week wildtype mice. The contribution of test and competitor cells was monitored by flow cytometry in the peripheral blood at 6 and 12 weeks and in the BM at 20 weeks post-transplant. The whole BM from primary recipients was then transplanted into lethally irradiated secondary CD45.1$^+$ recipients with donor contribution to the peripheral blood measured at 6 and 12 weeks and in the BM at 14 weeks post-transplant.

(B) Both female and male Smchd1-del BM show reduced reconstitution capacity compared with controls. The percentage of CD45.2$^+$ test cells in the PB (gated on B220$^+$ cells) and BM (gated on all CD45$^+$ cells) at the indicated time points post-BMT is shown as a proportion of all donor-derived cells. The dotted line indicates the expected percentage of CD45.2$^+$ cells, given the input proportion of test and competitor cells transplanted.

(C) The percentage of CD45.2$^+$ test cells contributing to the HSPC (LSK) compartment at 20 weeks post-transplant. A comparison between recipients receiving female or male Smchd1-del BM confirms a more severe reconstitution defect for female Smchd1-del BM cells.

(D) Secondary transplant recipients were monitored for reconstitution by CD45.2$^+$ donor-derived cells to the PB at 6 and 12 weeks post-BMT and the BM at 14 weeks post-BMT. Statistical comparisons between groups with different genotypes was performed in Prism 9 using the ordinary one-way ANOVA analysis with Sidak's multiple comparisons test. *$p < 0.05$, **$p < 0.01$, ***$p < 0.001$. All error bars represent SEM.

In contrast, there was a significant reduction in the percentage of CD45.2$^+$ test cells present in recipients that received either female or male Smchd1-del donor cells from as early as 6 weeks post-transplant in the peripheral blood, continuing at 12 and 20 weeks post-transplant (Figure 2B). These data indicate that both

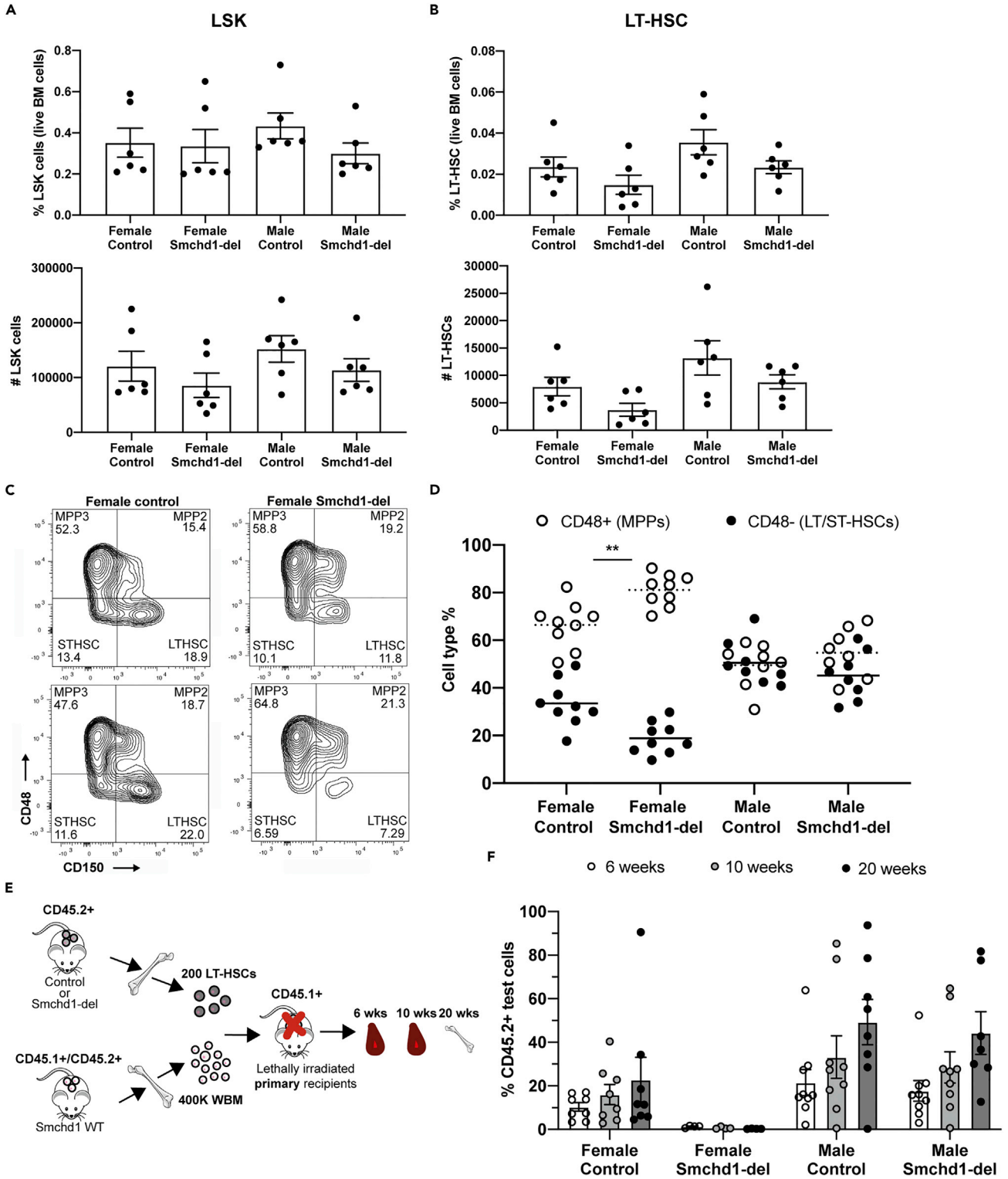

Figure 3. SMCHD1 is required for a normal HSPC compartment in female mice

(A and B) No significant differences in either the proportion or number of LSKs (A) or LT-HSCs (B) were observed between control and Smchd1-del mice. Data are from two independent experiments with six age-matched mice (5–8 months old) per group. Cell numbers are from two tibiae and two femurs.

(C) Representative flow cytometry plots gated on LSK Flt3$^-$ cells show different CD48 and CD150 staining profiles between two age-matched pairs of control and Smchd1-del female mice.

Figure 3. *Continued*

(D) Graph showing the proportion of CD48$^+$ MPPs and CD48$^-$ HSCs gated on LSK Flt3$^-$ cells illustrates altered CD48 expression within the Smchd1-del female HSPC population. Dotted lines represent the mean percentage for CD48$^+$ MPPs, and solid lines represent the mean percentage for CD48$^-$ HSCs.
(E) LT-HSCs (Lin$^-$ ckit$^+$ Sca1$^+$ Flt3$^-$ CD48$^-$ CD150$^+$) from control or Smchd1-del CD45.2$^+$ mice were transplanted into lethally irradiated CD45.1$^+$ recipient mice in competition with 4 × 10^5 wildtype CD45.1$^+$/CD45.2$^+$ whole BM cells. The contribution of test and competitor cells was monitored by flow cytometry in the peripheral blood and BM post-transplant.
(F) Contribution of CD45.2$^+$ cells to the peripheral blood at 6 and 10 weeks post-transplant and the BM at 20 weeks post-transplant. Statistical comparisons between groups with different genotypes was performed in Prism 9 using the ordinary one-way ANOVA analysis with Sidak's multiple comparisons test. *p < 0.05, **p < 0.01, ***p < 0.001. Graphs show the mean with error bars showing SEM.

short- and long-term reconstitution capacity is impaired in the absence of SMCHD1 (Figure 2B). We observed reduced contribution of Smchd1-del test cells to both lymphoid and myeloid cell populations in the peripheral blood (Figure S2A) and across all cell types analyzed in the thymus, spleen, and bone marrow at 20 weeks post-transplant (Figure S2B), including in the HSPC compartment where the reconstitution defect was significantly more pronounced in recipients of Smchd1-del female bone marrow compared with male cells (Figure 2C).

These data may indicate an inability of Smchd1-del HSPCs to properly home to the bone marrow niche post-transplantation. Competitive reconstitution assays analyzed at 18 h post-transplantation showed no significant difference in the proportion of Smchd1-del or control lineage$^-$ donor cells present in recipient bone marrow (Figure S2C). This suggests that *Smchd1*-deletion does not pose a major impediment to the homing capacity of immature bone marrow cells; however, we cannot conclude that this is the case for all HSPC subpopulations.

To further investigate the competitive reconstitution defect, we performed secondary transplants with 5 × 10^6 whole BM cells harvested from primary transplant recipients of female donor test cells (Figure 2A). In these secondary recipients, the ratio of CD45.2$^+$ test to CD45.1$^+$/CD45.2$^+$ competitor cells observed in the HSPC compartment of primary recipients was maintained (Figures 2D, S2D, and S2E). These data support a cell-autonomous role for SMCHD1 in maintaining a functional HSPC compartment.

SMCHD1 is required for a normal HPSC compartment in female mice

This observation prompted us to examine whether there was an alteration in the number or proportion of HSCs and different subsets of multipotent progenitors (MPPs) in the BM of Smchd1-del mice (Figure S3A) (Pietras et al., 2015; Wilson et al., 2008). We observed no significant difference in the number or proportion of HSPC-enriched LSK cells between different genotypes (Figure 3A), nor was there a significant difference in the total number of LT-HSCs or their proportion of total live BM cells (Figure 3B). Comparable LT-HSC numbers between genotypes were also seen using an alternative HSC/progenitor gating strategy (Figures S3A and S3B) (Oguro et al., 2013). There was no significant difference in the number or proportion of ST-HSCs or other MPP subsets (Figure S3C). We did note, however, that the CD48/CD150 flow cytometry staining profile within the LSK Flt3$^-$ population was altered to varying degrees in individual Smchd1-del females, with some Smchd1-del females showing a dramatic reduction in the proportion of CD48$^-$ HSCs, whereas others looked similar to matched controls (Figure 3C). When HSPC subsets were grouped based on CD48 expression, we observed a significant reduction in the proportion of CD48$^-$ HSCs and an increase in CD48$^+$ MPPs in Smchd1-del females (Figure 3D).

We next addressed whether the competitive reconstitution defect was owing to the subtle changes in the proportions of HSCs and thus the number transplanted in 2 × 10^6 total BM cells (estimated in Figure S3D). We transplanted 200 sorted LT-HSCs in competition with 4 × 10^5 whole BM cells (Figure 3E). Flow cytometry analysis showed no contribution of female Smchd1-del LT-HSCs to the peripheral blood or bone marrow of recipient animals, whereas male Smchd1-del LT-HSCs contributed at similar levels to controls (Figure 3F). We also saw no CD45.2$^+$ female Smchd1-del cells within the LT-HSC population of recipient mice (Figure S3E). These data suggest that both HSC number and function are affected by *Smchd1* deletion in females.

SMCHD1 is required for age-related expansion of HSCs

Aging is another stress on the hematopoietic system, with several changes in hematopoiesis commonly associated with increased age. These include a reduced number of lymphocytes in favor of increased

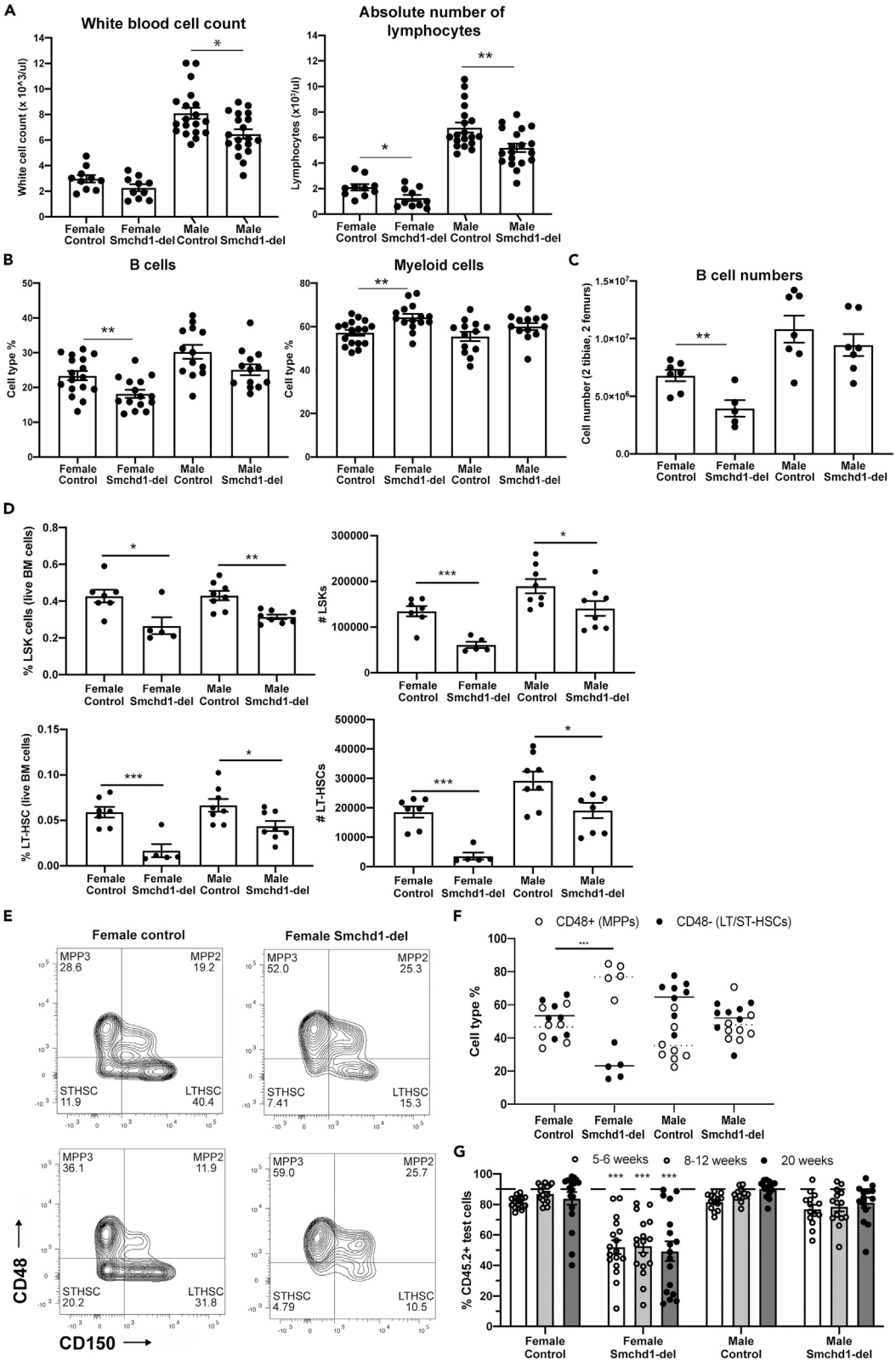
A
White blood cell count
White cell count (x 10^3/ul)
Absolute number of lymphocytes
Lymphocytes (x10^3/ul)
Female Control
Female Smchd1-del
Male Control
Male Smchd1-del
B
B cells
Cell type %
Myeloid cells
C
B cell numbers
Cell number (2 tibiae, 2 femurs)
D
% LSK cells (live BM cells)
# LSKs
% LT-HSC (live BM cells)
# LT-HSCs
E
Female control
Female Smchd1-del
MPP3
MPP2
STHSC
LTHSC
CD48
CD150
F
CD48+ (MPPs)
CD48- (LT/ST-HSCs)
Cell type %
G
5-6 weeks
8-12 weeks
20 weeks
% CD45.2+ test cells

Figure 4. SMCHD1 is required for age-related HSCs expansion

(A) White blood cell and lymphocyte numbers are reduced in the peripheral blood of aged Smchd1-del mice.

(B) Aged Smchd1-del female mice show altered cell proportions in the bone marrow with a decrease in the proportion of $B220^+$ B lymphocytes and an increase in $Mac1^+/CD11b^+$ myeloid cells.

(C) Aged Smchd1-del females have reduced numbers of $B220^+$ B cells in the bone marrow compared with controls.

(D) Both the proportion and number of HSPC-enriched LSK cells and LT-HSCs were reduced in aged Smchd1-del female and male mice compared with controls. Cell numbers are from two tibiae and two femurs.

(E) Representative flow cytometry plots gated on LSK $Flt3^-$ cells show altered CD48 and CD150 staining profiles between control and Smchd1-del female mice.

(F) Graph showing the proportion of $CD48^+$ MPPs and $CD48^-$ HSCs gated on LSK $Flt3^-$ cells.

(G) Aged Smchd1-del female but not male mice show reduced reconstitution capacity compared with controls. The percentage of $CD45.2^+$ test cells in the peripheral blood at 5–6 and 8–12 weeks post-transplant and in the bone marrow at 20 weeks post-transplant is shown as a proportion of all donor-derived cells. Statistical comparisons between groups with different genotypes was performed in Prism 9 using the ordinary one-way ANOVA analysis with Sidak's multiple comparisons test. *$p < 0.05$, **$p < 0.01$, ***$p < 0.001$. Graphs show mean with error bars indicating SEM.

myeloid cell numbers, increased incidence of malignancies, and a clonal expansion of LT-HSCs that have a suboptimal function (Dykstra et al., 2011; Goodell and Rando, 2015; Sun et al., 2014).

We analyzed 12- to 18-month-old mice to determine whether a healthy hematopoietic system was maintained during aging in the absence of SMCHD1. *Smchd1* deletion did not lead to hematological malignancy in mice monitored for over one year; however, similar to younger Smchd1-del mice there was a reduction in peripheral blood lymphocyte numbers (Figure 4A), whereas myeloid cell numbers were comparable with controls (Figure S4A). We observed a skewing of cell-type proportions in the blood (Figure S4B) and bone marrow (Figure 4B) of aged Smchd1-del females with reduced B cell and increased myeloid cell proportions, owing to a significant reduction in the number of B cells (Figure 4C), whereas overall bone marrow and myeloid cell numbers were maintained (Figure S4C).

Examination of the HSPC compartment by flow cytometry showed a significant reduction in the proportion and number of LSKs and LT-HSCs, as well as reduced numbers of ST-HSCs in both male and female aged Smchd1-del mice compared with controls (Figures 4D and S4D). We also saw reduced numbers of myeloid-primed MPP3 and lymphoid-primed MPP4 progenitors in aged female Smchd1-del mice (Figure S4D). The flow cytometry staining profile for CD48 and CD150 was altered in aged Smchd1-del females, with a reduction in the proportion of $CD48^-$ HSCs, reminiscent of what is observed in some young Smchd1-del females, rather than the expansion of this population that is normally evident in older animals (Figures 4E and 4F).

We tested the reconstitution capacity of aged Smchd1-del BM by performing competitive BM transplants as described earlier (Figure 2A). We found that transplant of aged Smchd1-del female bone marrow showed a similar phenotype as that in younger mice, with a reduced contribution of $CD45.2^+$ test cells observed at early and late time-points post-transplantation (Figure 4G). As shown above, we observed a 3.5-fold reduction in the proportion of LT-HSCs present in the bone marrow of Smchd1-del females compared with controls, which would alter our 10:1 competitive transplant closer to a 3:1 ratio, meaning we would expect a 75% contribution rather than 90%, which is still higher than the mean 50% contribution that we observed. Aged Smchd1-del male BM was not significantly less competitive than controls (Figure 4G); this may be because even in *Smchd1*-deleted males the proportion of LT-HSCs in the BM is higher in aged mice ($0.044 \pm 0.016\%$) than younger mice ($0.023 \pm 0.008\%$), such that on average twice as many LT-HSCs are being transplanted from aged donors. Despite the reduced repopulating capacity of aged HSCs, the increased number of LT-HSCs transplanted at a 10:1 test to competitor cell ratio may saturate the system, making it difficult to distinguish subtle deficiencies. These data show a role of SMCHD1 in age-related HSC maintenance, which is most pronounced in females.

Expression profiling of *Smchd1*-deleted hematopoietic cells shows upregulation of known autosomal targets and dysregulation of X-linked genes in females

We next sought to examine how *Smchd1* deletion affects gene expression in hematopoietic cells. We performed low input RNA sequencing on HSCs by sorting replicate samples of 50–100 LSK $Flt3^-$ $CD48^-$ $CD150^+$ LT-HSCs from three individual Smchd1-del females and corresponding age-matched controls (2.5- to 6-months old). We observed 5 significantly upregulated genes and 40 downregulated genes in our Smchd1-del LT-HSCs, although there was some variation between the three Smchd1-del individuals (Figure 5A, S5A and Table S2). Whereas we confirmed that *Smchd1* expression is indeed reduced, we

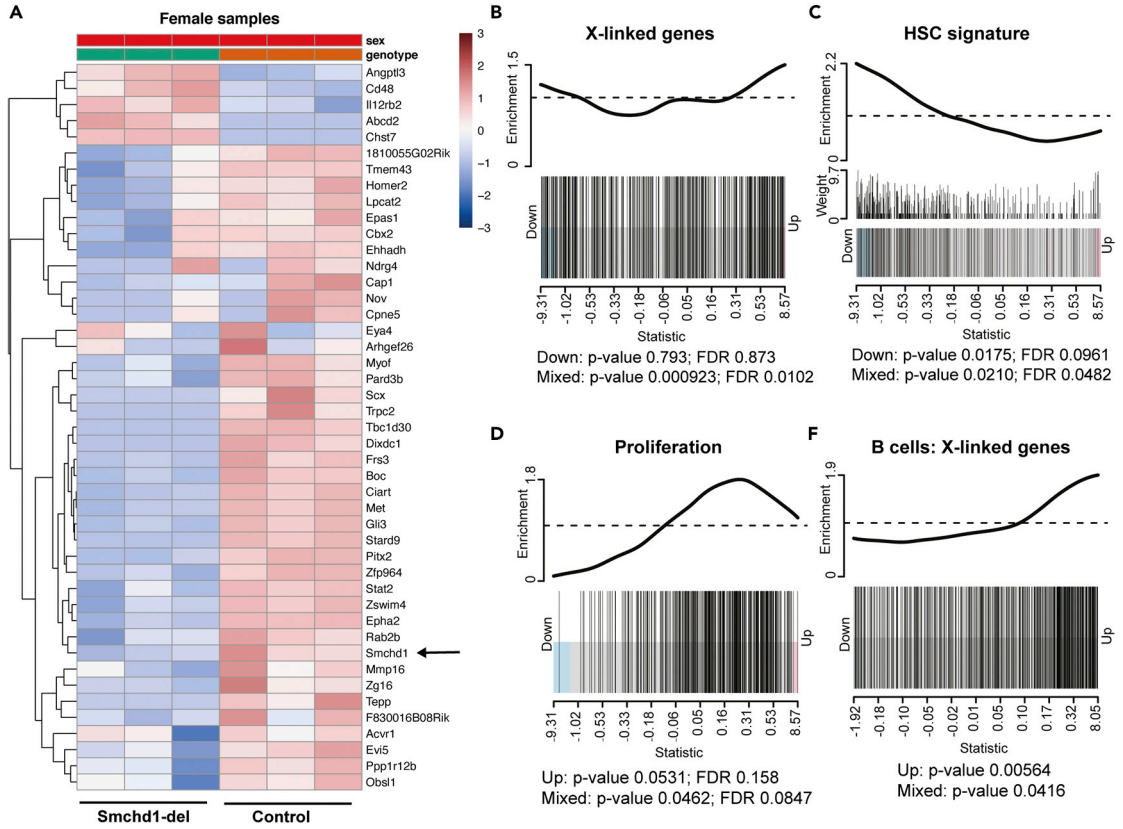
A
Female samples
sex
genotype
Angptl3
Cd48
Il12rb2
Abcd2
Chst7
1810055G02Rik
Tmem43
Homer2
Lpcat2
Epas1
Cbx2
Ehhadh
Ndrg4
Cap1
Nov
Cpne5
Eya4
Arhgef26
Myof
Pard3b
Scx
Trpc2
Tbc1d30
Dixdc1
Frs3
Boc
Ciart
Met
Gli3
Stard9
Pitx2
Zfp964
Stat2
Zswim4
Epha2
Rab2b
Smchd1
Mmp16
Zg16
Tepp
F830016B08Rik
Acvr1
Evi5
Ppp1r12b
Obsl1
Smchd1-del
Control
B
X-linked genes
Enrichment
Down
Up
Statistic
Down: p-value 0.793; FDR 0.873
Mixed: p-value 0.000923; FDR 0.0102
C
HSC signature
Enrichment
Weight
Down
Up
Statistic
Down: p-value 0.0175; FDR 0.0961
Mixed: p-value 0.0210; FDR 0.0482
D
Proliferation
Enrichment
Down
Up
Statistic
Up: p-value 0.0531; FDR 0.158
Mixed: p-value 0.0462; FDR 0.0847
F
B cells: X-linked genes
Enrichment
Down
Up
Statistic
Up: p-value 0.00564
Mixed: p-value 0.0416
E
Young females
Aged females
% gated on LT-HSCs
Female Control
Female Smchd1-del
G0
G1
G2M
S
Control
Smchd1-del
CD48
CD150
LT-HSC
8.86
9.89
25.4
7.06
Ki67
DAPI
G1 48.8
S 4.64
G2M 8.05
G0 37.6
G1 73.4
S 6.58
G2M 8.22
G0 9.87
G1 22.6
S 4.02
G2M 4.70
G0 67.3
G1 56.7
S 8.10
G2M 8.80
G0 24.6

Figure 5. SMCHD1 is required for appropriate regulation of the X chromosome and autosomal genes in HSCs and B lymphocytes

(A) Heatmap of upper-quartile-normalized logCPM values for differentially expressed genes between female Smchd1-del and control HSCs.

(B) Barcode plot for X chromosome gene set tested in the Smchd1-del HSC compared with control HSC data set. Genes are represented by bars and are ranked from the left to right by increasing the log-fold change. For all the barcode plots shown here, the line above the barcode shows the relative local enrichment of the vertical bars in each part of the plot. The dotted horizontal line indicates neutral enrichment; the line above the dotted line shows enrichment, whereas the line below the dotted line shows depletion.

(C) Barcode plot for the HSC signature gene set tested in the Smchd1-del HSC compared with control HSC data set. Genes in this set have enriched expression in HSCs compared with other hematopoietic cell types merged from two separate studies (Chambers et al., 2007a; Gazit et al., 2013). Directional barcode plot "weights" are given by the logFC of the genes within in the Chambers et al. gene set.

(D) Barcode plot for the HSC proliferation gene set (Venezia et al., 2004) tested in the Smchd1-del HSC compared with the control HSC data set.

(E) Cell cycle analysis of LT-HSCs from young and aged female mice. Graphs show the mean ± SEM. Statistical comparisons between groups with different genotypes was performed in Prism 9 using the ordinary one-way ANOVA analysis with Sidak's multiple comparisons test. *$p < 0.05$, ***$p < 0.001$, ****$p < 0.0001$. Error bars indicate SEM. Representative flow cytometry plots show staining for $CD48^-$ $CD150^+$ LT-HSCs gated on Lin^- $Sca1^+$ $ckit^+$ cells and Ki67 and DAPI staining within the LT-HSC population to determine cell cycle stage.

(F) Barcode plot for X chromosome gene set tested in the Smchd1-del B cells compared with the control B cells data set. For all barcode plots a significant "Up" p-value means that the differential expression results found in the RNA-seq data are positively correlated with the expression signature from the corresponding gene set. Conversely, a significant "Down" p-value means that the differential expression log-fold-changes are negatively correlated with the expression signature from the corresponding gene set. A significant "Mixed" p-value means that the genes in the set tend to be differentially expressed without regard for direction.

did not observe upregulation of known autosomal SMCHD1 target genes, such as genes of the Prader-Willi Syndrome imprinted cluster.

As SMCHD1 has a pivotal role in X chromosome inactivation, and the phenotypes we observed are much stronger in females, we next sought to determine whether loss of SMCHD1 in HSCs leads to general de-repression of X-linked genes. Whereas we saw the significant upregulation of the X-linked gene *Chst7*, there was no widespread upregulation of X-linked transcripts in Smchd1-del HSCs. However, gene set testing revealed statistically significant disruption to the expression of genes on the X chromosome between Smchd1-del and control HSCs (FDR 0.010), although, surprisingly, the direction of the change was not consistent (Figure 5B).

We performed further gene set testing for specific sets of genes related to HSC identity and function. A set of HSC signature genes taken from publications identifying genes with enriched expression in HSCs compared with other hematopoietic cell types (Chambers et al., 2007a; Gazit et al., 2013) were significantly dysregulated between Smchd1-del and control HSCs (p-value 0.019; FDR 0.048). Although not significant (p-value 0.017; FDR 0.096), the fold-changes were predominantly negatively correlated with the expression signature from the HSC gene set, suggesting that HSC identity is reduced with *Smchd1* deletion (Figure 5C). We tested whether Smchd1-del HSC has acquired transcriptional changes associated with aging by testing for the enrichment of genes that are differentially expressed between young and aged HSCs (Sun et al., 2014). Whereas we again observed significant dysregulation of these (p-value 0.002; FDR 0.014), there was no significant directional correlation to indicate that Smchd1-del HSCs resemble aged HSCs (Figure S5B).

We looked at gene sets associated with HSC quiescence and proliferation (Venezia et al., 2004), whereas there was no enrichment for quiescence-associated genes (Figure S5C), we saw dysregulation of genes within the proliferation gene set (p-value 0.021; FDR 0.048) (Figure 5D). Although not significant (p-value 0.053; FDR 0.133), genes associated with HSC proliferation were predominantly positively correlated with the observed gene expression changes. Among the SMCHD1-sensitive genes identified in HSCs were several with known roles in HSC proliferation. We saw upregulation of *Cd48* gene expression in Smchd1-del HSCs, which mirrors the flow cytometry staining profile observed in Smchd1-del females. CD48 has been shown to modulate HSC activity by altering the cytokine milieu, with high levels of CD48 marking cycling HSCs, whereas the loss of *CD48* inhibits HSC proliferation under steady-state conditions (Boles et al., 2011; Venezia et al., 2004). ANGPTL3 was also increased and has similarly been implicated in stimulating HSC proliferation and expansion (Zhang et al., 2006; Zheng et al., 2011). The increased expression of these genes may indicate that Smchd1-del HSCs are in a more proliferative state.

In light of this, we sought to determine whether *Smchd1*-deletion alters cell cycle parameters in LT-HSCs. We observed an increased proportion of LT-HSCs in G_1 and a reduced proportion in the quiescent G_0 stage in both young and aged Smchd1-del females (Figure 5E), a change not evident in aged Smchd1-del males

(Figure S5D). These data suggest that SMCHD1 has a role in cell cycle regulation in maintaining quiescence and restricting proliferation in female LT-HSCs, and may thereby protect against HSC exhaustion and a loss of this population with age.

Detection of altered expression in very low input samples can be challenging, particularly when we expect based on prior data in other cell types to observe genes that are normally switched off to be upregulated upon *Smchd1* deletion; something that is difficult to confidently detect in samples with high rates of dropout. To further examine how *Smchd1* deletion affects expression in the blood system and overcome some of these limitations, we performed RNA sequencing on $B220^+$ B cells sorted from the bone marrow of aged (12- to 16-month old) Smchd1-del mice alongside matched controls. The reduced proportion of B lymphocytes in the peripheral blood of younger *Smchd1*-deleted females, and the reduction in their number and proportion in aged females, suggested a functional role for SMCHD1 in B cell development or maintenance.

We found 35 genes that were differentially expressed between female Smchd1-del and control B cells compared with 16 between males, with *Smchd1* the only significantly downregulated gene in Smchd1-del B cells (Figures S5E and S5F). Genes from the Prader-Willi Syndrome imprinted cluster, *Peg12* and *Mkrn3,* were upregulated in both female and male Smchd1-del B cells, as was the clustered protocadherin gene, *Pcdha10* (Tables S3 and S4), showing that SMCHD1 is important in regulating their expression across several different cell types (Chen et al., 2015; Jansz et al., 2018; Leong et al., 2013; Wang et al., 2018).

We found *Prospero homeobox gene 1 (Prox1)* to be the most significantly upregulated gene in female and male Smchd1-del B cells. PROX1 has an important role in lymphatic epithelial cell development (Wigle et al., 2002; Wigle and Oliver, 1999) and has previously been identified as a moderator of HSC activity, with reduced *Prox1* levels enhancing HSC function, whereas forced overexpression in an HSC culture system leads to a loss of *Prox1*-overexpressing cells (Hope et al., 2010). Expression of *Prox1* was not detected in our low input HSC RNA sequencing; however, we observed increased expression of *Prox1* in Smchd1-del HSPC-enriched $lineage^-$ $ckit^+$ BM cells by RT-qPCR (Figure S5G), suggesting that *Prox1* may indeed be overexpressed in stem cells where it could impact repopulation capacity.

We next sought to determine whether X chromosome inactivation was compromised in female B cells lacking SMCHD1. Gene set testing showed that X-linked genes tend to be upregulated in Smchd1-del B cells compared with controls (p-value 0.006) (Figure 5F). Whereas we are unable to confirm that this is owing to the upregulation of genes on the inactive X chromosome, it does suggest a role for SMCHD1 in maintaining X chromosome gene repression in female B cells.

DISCUSSION

Here we report a role for SMCHD1 in regulating hematopoietic stem cell (HSC) function, a role that is more pronounced in female mice. We utilized a *Vav.Cre* transgenic mouse line (Croker et al., 2004; Ogilvy et al., 1999) to conditionally delete *Smchd1* within the blood cell lineage and observed fewer than expected $Smchd1^{del/fl}$ $Vav.Cre^{T/+}$ female mice in our colony at weaning. Similar to other reported *Vav* transgenic lines, this *Vav.Cre* transgene is known to express and promote recombination in all blood cell lineages (Croker et al., 2004; de Boer et al., 2003; Georgiades et al., 2002; Stadtfeld and Graf, 2005) with limited expression also observed in other tissues (Croker et al., 2004; Ogilvy et al., 1999), whereas endogenous *Vav* expression has also been noted in placental trophoblast cells (Zmuidzinas et al., 1995). Therefore, the lower-than-expected numbers of $Smchd1^{del/fl}$ $Vav.Cre^{T/+}$ females could either be owing to incomplete penetrance of lethality caused by *Smchd1* deletion in blood cells or variable promiscuous deletion of *Smchd1* in other non-hematopoietic tissues, such as the placenta where SMCHD1 is involved in imprinted X chromosome inactivation in females (Blewitt et al., 2008).

In the steady state, we found that *Vav.Cre* transgene-driven deletion of *Smchd1* leads to minimal phenotypic changes in young mice beyond reduced peripheral blood lymphocyte numbers, specifically B lymphocytes in the females. There was a significant reduction in B cell numbers within the bone marrow of aged *Smchd1*-deleted females, with the normal age-related skewing in cell proportions owing to decreased lymphocyte and increased myeloid cell production (de Haan and Lazare, 2018; Rossi et al., 2005) more pronounced in *Smchd1*-deleted females. *Smchd1*-deleted mice appeared otherwise well; they had a normal lifespan with no indications of hematological malignancies. Along with the peripheral

blood analysis of *Smchd1*-null males harboring a nonsense (*MommeD1*) mutation, these data suggest that at rest, SMCHD1 is not strictly required to maintain a healthy hematopoietic system.

The effect of *Smchd1* deletion became evident when HSCs were forced to perform under the stress of competitive bone marrow reconstitution. Both *Smchd1*-deleted male and female bone marrow competed poorly against *Smchd1*$^{+/+}$ competitor cells despite the high input proportion of test cells, with the defect in repopulating capacity more pronounced for *Smchd1*-deleted female donors. Whereas the number of cell surface marker-defined HSCs was not significantly reduced in younger *Smchd1*-deleted animals, *Smchd1*-deleted females showed an increased proportion of CD48^{+} multipotent progenitors and a decrease in CD48^{-} HSCs, indicating a disrupted HSPC compartment. This is further evidenced by the altered cell cycle dynamics within the female *Smchd1*-deleted LT-HSCs, with a reduced number of cells in the G_0 stage and an increase in G_1, suggesting a role for SMCHD1 in maintaining HSC quiescence.

In aged mice, the reduction in HSC number and proportion was significant, and again more striking in females. An increase in HSC number and frequency is a hallmark of the aged hematopoietic system, although these aged HSCs are functionally impaired (Chambers et al., 2007b; Dykstra et al., 2011; Rossi et al., 2005); this normal HSC expansion was not evident in *Smchd1*-deleted females. Whereas there was an increase in HSC number and proportion in *Smchd1*-deleted males with age, this was still significantly lower than controls, and unlike in aged females, we did not observe any significant alterations to the cell cycle. These data indicate a role for SMCHD1 in age-related HSC maintenance and expansion.

Whereas fewer transplanted HSCs may partially account for the reduced test cell chimerism seen in recipients of female *Smchd1*-deleted bone marrow, we saw no contribution of female *Smchd1*-deleted cells when defined numbers of sorted LT-HSCs were transplanted in a competitive setting, questioning whether these cells retain normal HSC function in the absence of SMCHD1; indeed, a negative correlation with the HSC signature gene set suggests that *Smchd1*-deleted cells may be less HSC-like. We also identified *Prox1*, which has been proposed to promote HSPC commitment and differentiation (Hope and Sauvageau, 2011), as an SMCHD1-sensitive gene, with *Prox1* upregulation in *Smchd1*-deleted progenitor cells potentially compromising their stemness. Whereas we saw no evidence that the homing capacity of lineage^{-} bone marrow cells was impaired in the absence of SMCHD1, this doesn't exclude the possibility that *Smchd1*-deleted LT-HSCs may fail to home to the bone marrow.

We did, however, see the contribution of female *Smchd1*-deleted cells in secondary whole bone marrow transplant recipients and when using aged donors, indicating that SMCHD1 is not absolutely required for long-term repopulating capabilities; however, this capacity may not reside within the marker-defined LT-HSC population. A study examining lysine acetyltransferase KAT6A found no defect in homeostatic hematopoiesis despite significantly reduced numbers of HSCs, and whereas bone marrow from mice in which *Kat6a* had been deleted 15 months prior showed engraftment defects in a competitive setting, *Kat6a*-deleted donor cells showed substantial long-term contribution to recipients in non-competitive reconstitutions (Sheikh et al., 2016). These observations suggest that over the lifetime of an animal, cells lacking the cell surface markers that define the HSC-enriched population may have acquired self-renewal capacity (Sheikh et al., 2016), which could account for the continued contribution of female *Smchd1*-deleted cells in secondary transplants.

HSC loss after hematopoietic stress and a failure to maintain HSCs in the bone marrow are features of compromised quiescence (Ficara et al., 2008; Gudmundsson et al., 2020). Whereas genes associated with HSC quiescence do not appear to be dysregulated in female Smchd1-del HSCs, we do see a reduction of *Smchd1*-deleted LT-HSCs within the quiescent G_0 stage of the cell cycle both in young and aged females. We also see a positive correlation with proliferation associated genes. *Cd48* was identified as an SMCHD1-sensitive gene, with increased *Cd48* gene expression and an increased proportion of CD48^{+} HSPCs. Although CD48 expression is excluded from primitive LT-HSCs, stimulating HSCs to cycle using 5-flurouracil causes transient upregulation of *Cd48* expression, with substantially higher levels of CD48 detected by flow cytometry at the peak of HSC proliferation after treatment (Venezia et al., 2004). Female *Smchd1*-deleted HSCs also upregulate *Angptl3*, which has been shown to stimulate HSC expansion; *Angptl3*-null HSCs show lower repopulating capacity, whereas forced expression of ANGPTL3 in lineage^{-} BM cells leads to a moderate increase in recipient chimerism (Farahbakhshian et al., 2014; Zhang et al., 2006; Zheng et al., 2011). These data suggest a role for SMCHD1 in cell cycle regulation whereby it

maintains HSC quiescence and thus self-renewal, and restricts proliferation. The loss of HSCs from the G_0 fraction in the absence of SMCHD1 could impact long-term reconstitution capacity, given that the engraftment potential of HSCs predominantly resides within the G_0 fractions (Passegué et al., 2005), and this could lead to premature exhaustion of HSCs as they more readily differentiate into multipotent progenitors.

Whereas we do see a shift in the proportion of HSCs in favor of multipotent progenitors, the number of MPPs is reduced in Smchd1-del female mice compared with controls. In zebrafish, *smchd1* knockdown results in reduced HSPC numbers and a reduced proportion of proliferating blood cells, causing disruption to definitive hematopoiesis and pointing to a role for SMCHD1 in HSPC expansion (Xue et al., 2019). Our data also suggest that SMCHD1 is required for HSC expansion in mice.

Given the established role for SMCHD1 in the female-specific process of X chromosome inactivation (Blewitt et al., 2008), we sought to determine whether the differing phenotypic severity observed between the sexes was owing to dysregulated X-linked gene expression in female HSCs. It is important to note that the loss of *Smchd1* may also be more detrimental to female HSCs given innate differences between males and females that affect HSC activity and could influence the varying phenotype we observed between the sexes (Liu et al., 2011). For example, the sex hormone estrogen has been shown to influence HSC self-renewal, with female HSCs shown to divide more frequently than male HSCs with the possibility that this increased proliferation could lead to premature HSC exhaustion in females (Leeman and Brunet, 2014; Nakada et al., 2014). Here though we focused on examining X-linked gene expression changes.

We saw a significant change in X-linked genes when considered as a gene set, although we did not detect wholesale upregulation of X-linked transcripts in *Smchd1*-deleted HSCs; however, such upregulation may not be expected in this context. Studies have shown that ablation of SMCHD1 after X inactivation is complete, which results in changes to chromatin conformation of the inactive X (Xi) chromosome but not to reactivation of Xi genes, whereas *Smchd1* deletion before X inactivation results in expression of Xi genes (Gdula et al., 2019; Jansz et al., 2018; Sakakibara et al., 2018; Wang et al., 2018, 2019). Still, the expression level of these upregulated Xi genes does not often reach that seen on the active X chromosome and not all X-linked genes are sensitive to SMCHD1 loss (Gdula et al., 2019; Gendrel et al., 2012; Jansz et al., 2018). Deletion of *Smchd1* in our system likely occurred by embryonic day 11.5 in c-kit$^+$ HSPCs in the fetal liver (Perez-Cunningham et al., 2016), after X inactivation is complete and multiple epigenetic mechanisms have locked in this state. Furthermore, a study examining the outcome of blood-specific deletion of *Xist*, the long non-coding RNA strictly required for X chromosome inactivation, found very few differentially expressed X-linked transcripts in *Xist*-deficient female HSCs, despite defects in HSC number and function, and the development of a highly aggressive and fully penetrant myeloproliferative disease in female mice (Yildirim et al., 2013). It is possible there are rare cases of X chromosome reactivation in *Smchd1*-deleted LT-HSCs, but this would not be detectable using low input gene expression profiling or likely single-cell RNAseq owing to the high dropout rate for lowly expressed genes. It is interesting to note that the HSC phenotype is variable between *Smchd1*-deleted females, with highly variable numbers of LT-HSCs sorted from individual mice. It is possible that *Smchd1* deletion is also having a variable effect within individual HSCs. Unlike the loss of a transcription factor that directly controls a defined set of downstream target genes, ablation of SMCHD1 may prime cells for variegated expression changes. Indeed, we may be measuring the function and gene expression changes of those cells that were able to survive and thus least affected by *Smchd1* loss.

Inactivation of the X chromosome has been shown to become impaired in aged HSCs, with age-related erosion of LaminA/C-associated repressive nuclear compartments and increases in chromatin accessibility leading to more highly variable expression of X-linked transcripts in aged HSCs compared with their younger counterparts (Grigoryan et al., 2021). We found that X chromosome genes tended to be differentially expressed between *Smchd1*-deleted and control HSCs by gene set testing, although the directionality of the effect was not always upregulation of these genes as might be expected when removing a repressor protein. Taken together, our data suggest a destabilized X chromosome in Smchd1-del HSCs.

In B cells from aged females, we also see a dysregulation of X-linked genes in the absence of SMCHD1, but in this case, it is a significant upregulation of X-linked genes. Lymphocytes are particularly interesting given the unusual way in which the Xi is maintained; in the B cell lineage, there is a reduction in *Xist* RNA marking the Xi from the pro-B cell stage of development with a gradual loss of repressive histone marks at the Xi

throughout differentiation until activation of mature B cells leads to relocalization of *Xist* RNA to the Xi (Syrett et al., 2017; Wang et al., 2016). Given the eroded X inactivation state in resting B cells, SMCHD1's role in maintaining gene silencing may be enhanced, which could explain why X-linked genes are upregulated in this context. In future, it would be interesting to determine whether SMCHD1 also has a role in reestablishing X inactivation upon lymphocyte activation. That X chromosome genes tend to be differentially expressed between *Smchd1*-deleted and control HSCs and B cells, along with the strong phenotype in females, suggests that SMCHD1 is important for preventing epigenetic deregulation of the X chromosome.

Taken together with the role of SMCHD1 in other cell types, we predict that SMCHD1 is required to maintain chromatin conformation in HSCs, which have been shown to have unique higher-order chromatin structures (Zhang et al., 2020). This role appears most pronounced in females, potentially owing to the effect on the inactive X chromosome. In conclusion, we have shown that in mice, SMCHD1 is not required for steady-state hematopoiesis but plays an important role in the maintenance of adult HSCs, particularly in females.

Limitations of the study

We employed a *Vav.Cre* transgenic mouse model to conditionally delete *Smchd1* within the hematopoietic system. Whereas the *Vav.Cre* transgene has been shown to successfully induce the recombination of *floxed* alleles throughout the hematopoietic system early in embryonic development, it is also expressed in endothelial and germline cells (Croker et al., 2004; de Boer et al., 2003; Georgiades et al., 2002; Ogilvy et al., 1999; Perez-Cunningham et al., 2016). Whereas whole bone marrow and LT-HSC transplantation assays confirm a cell-autonomous role for SMCHD1 in the hematopoietic system, we cannot exclude that *Smchd1* deletion in non-hematopoietic cells may affect the steady-state phenotype in unmanipulated animals.

STAR★METHODS

Detailed methods are provided in the online version of this paper and include the following:

- KEY RESOURCES TABLE
- RESOURCE AVAILABILITY
  - Lead contact
  - Material availability
  - Data and code availability
- EXPERIMENTAL MODEL AND SUBJECT DETAILS
  - Animal husbandry and ethics
  - *Smchd1*$^{GFP/GFP}$ mice
  - *Smchd1*- *Vav.Cre* mice
  - *Smchd1*^{MommeD1} mice
- METHOD DETAILS
  - Genotyping
  - Peripheral blood analysis
  - Hematopoietic organ analysis by flow cytometry
  - Cell cycle analysis
  - Competitive bone marrow transplantation assays
  - HSC minibulk RNA-Seq
  - HSC minibulk RNA-Seq analysis
  - B cell bulk RNA-Seq
  - Gene set testing
  - RT-qPCR
- QUANTIFICATION AND STATISTICAL ANALYSIS

SUPPLEMENTAL INFORMATION

Supplemental information can be found online at https://doi.org/10.1016/j.isci.2022.104684.

ACKNOWLEDGMENTS

We thank The Walter & Eliza Hall Institute Flow Cytometry Facility, SCORE, and Bioservices, in particular Jessica Martin, for help with animal procedures. MEB was supported by a Bellberry-Viertel Senior Medical Research Fellowship. This work was supported by grants from the National Health and Medical Research

Council of Australia to MEB (GNT1098290 and GNT1194345). This work was made possible through Victorian State Government Operational Infrastructure Support and Australian National Health and Medical Research Council Research Institute Infrastructure Support Scheme IRIISS grant (9000653).

AUTHOR CONTRIBUTIONS

S.A.K. and M.E.B. designed the experiments. S.A.K., J.L., T.B., K.A.B., M.I., and M.E.B. performed the experiments. P.H. and S.A.K. performed the bioinformatics analysis. S.A.K. and M.E.B. wrote the manuscript. All authors contributed to discussions and edited the manuscript.

DECLARATION OF INTERESTS

The authors declare no competing interests.

Received: November 17, 2021
Revised: May 16, 2022
Accepted: June 24, 2022
Published: July 15, 2022

REFERENCES

Bagger, F.O., Kinalis, S., and Rapin, N. (2019). BloodSpot: a database of healthy and malignant haematopoiesis updated with purified and single cell mRNA sequencing profiles. Nucleic Acids Res. *47*, D881–d885. https://doi.org/10.1093/nar/gky1076.

Blewitt, M.E., Gendrel, A.V., Pang, Z., Sparrow, D.B., Whitelaw, N., Craig, J.M., Apedaile, A., Hilton, D.J., Dunwoodie, S.L., Brockdorff, N., et al. (2008). SmcHD1, containing a structural-maintenance-of-chromosomes hinge domain, has a critical role in X inactivation. Nat. Genet. *40*, 663–669. https://doi.org/10.1038/ng.142.

Blewitt, M.E., Vickaryous, N.K., Hemley, S.J., Ashe, A., Bruxner, T.J., Preis, J.I., Arkell, R., and Whitelaw, E. (2005). An N-ethyl-N-nitrosourea screen for genes involved in variegation in the mouse. Proc. Natl. Acad. Sci. USA *102*, 7629–7634. https://doi.org/10.1073/pnas.0409375102.

Boles, N.C., Lin, K.K., Lukov, G.L., Bowman, T.V., Baldridge, M.T., and Goodell, M.A. (2011). CD48 on hematopoietic progenitors regulates stem cells and suppresses tumor formation. Blood *118*, 80–87. https://doi.org/10.1182/blood-2010-12-322339.

Bullard, J.H., Purdom, E., Hansen, K.D., and Dudoit, S. (2010). Evaluation of statistical methods for normalization and differential expression in mRNA-Seq experiments. BMC Bioinf. *11*, 94. https://doi.org/10.1186/1471-2105-11-94.

Chambers, S.M., Boles, N.C., Lin, K.Y.K., Tierney, M.P., Bowman, T.V., Bradfute, S.B., Chen, A.J., Merchant, A.A., Sirin, O., Weksberg, D.C., et al. (2007a). Hematopoietic fingerprints: an expression database of stem cells and their progeny. Cell Stem Cell *1*, 578–591. https://doi.org/10.1016/j.stem.2007.10.003.

Chambers, S.M., Shaw, C.A., Gatza, C., Fisk, C.J., Donehower, L.A., and Goodell, M.A. (2007b). Aging hematopoietic stem cells decline in function and exhibit epigenetic dysregulation. PLoS Biol. *5*, e201. https://doi.org/10.1371/journal.pbio.0050201.

Chen, K., Hu, J., Moore, D.L., Liu, R., Kessans, S.A., Breslin, K., Lucet, I.S., Keniry, A., Leong, H.S., Parish, C.L., et al. (2015). Genome-wide binding and mechanistic analyses of Smchd1-mediated epigenetic regulation. Proc. Natl. Acad. Sci. USA *112*, E3535–E3544. https://doi.org/10.1073/pnas.1504232112.

Chen, Y., Lun, A.T.L., and Smyth, G.K. (2016). From reads to genes to pathways: differential expression analysis of RNA-Seq experiments using Rsubread and the edgeR quasi-likelihood pipeline. F1000Res. *5*, 1438. https://doi.org/10.12688/f1000research.8987.2.

Croker, B.A., Metcalf, D., Robb, L., Wei, W., Mifsud, S., DiRago, L., Cluse, L.A., Sutherland, K.D., Hartley, L., Williams, E., et al. (2004). SOCS3 is a critical physiological negative regulator of G-CSF signaling and emergency granulopoiesis. Immunity *20*, 153–165. https://doi.org/10.1016/s1074-7613(04)00022-6.

de Boer, J., Williams, A., Skavdis, G., Harker, N., Coles, M., Tolaini, M., Norton, T., Williams, K., Roderick, K., Potocnik, A., and Kioussis, D. (2003). Transgenic mice with hematopoietic and lymphoid specific expression of Cre. Eur. J. Immunol. *33*, 314–325. https://doi.org/10.1002/immu.200310005.

de Greef, J.C., Krom, Y.D., den Hamer, B., Snider, L., Hiramuki, Y., van den Akker, R.F.P., Breslin, K., Pakusch, M., Salvatori, D.C.F., Slütter, B., et al. (2018). Smchd1 haploinsufficiency exacerbates the phenotype of a transgenic FSHD1 mouse model. Hum. Mol. Genet. *27*, 716–731. https://doi.org/10.1093/hmg/ddx437.

de Haan, G., and Lazare, S.S. (2018). Aging of hematopoietic stem cells. Blood *131*, 479–487. https://doi.org/10.1182/blood-2017-06-746412.

Dykstra, B., Olthof, S., Schreuder, J., Ritsema, M., and de Haan, G. (2011). Clonal analysis reveals multiple functional defects of aged murine hematopoietic stem cells. J. Exp. Med. *208*, 2691–2703. https://doi.org/10.1084/jem.20111490.

Eaves, C.J. (2015). Hematopoietic stem cells: concepts, definitions, and the new reality. Blood *125*, 2605–2613. https://doi.org/10.1182/blood-2014-12-570200.

Farahbakhshian, E., Verstegen, M.M., Visser, T.P., Kheradmandkia, S., Geerts, D., Arshad, S., Riaz, N., Grosveld, F., van Til, N.P., and Meijerink, J.P.P. (2014). Angiopoietin-like protein 3 promotes preservation of stemness during ex vivo expansion of murine hematopoietic stem cells. PLoS One *9*, e105642. https://doi.org/10.1371/journal.pone.0105642.

Ficara, F., Murphy, M.J., Lin, M., and Cleary, M.L. (2008). Pbx1 regulates self-renewal of long-term hematopoietic stem cells by maintaining their quiescence. Cell Stem Cell *2*, 484–496. https://doi.org/10.1016/j.stem.2008.03.004.

Gazit, R., Garrison, B., Rao, T., Shay, T., Costello, J., Ericson, J., Kim, F., Collins, J., Regev, A., Wagers, A., and Rossi, D. (2013). Transcriptome analysis identifies regulators of hematopoietic stem and progenitor cells. Stem Cell Rep. *1*, 266–280. https://doi.org/10.1016/j.stemcr.2013.07.004.

Gdula, M.R., Nesterova, T.B., Pintacuda, G., Godwin, J., Zhan, Y., Ozadam, H., McClellan, M., Moralli, D., Krueger, F., Green, C.M., et al. (2019). The non-canonical SMC protein SmcHD1 antagonises TAD formation and compartmentalisation on the inactive X chromosome. Nat. Commun. *10*, 30. https://doi.org/10.1038/s41467-018-07907-2.

Gendrel, A.V., Apedaile, A., Coker, H., Termanis, A., Zvetkova, I., Godwin, J., Tang, Y., Huntley, D., Montana, G., Taylor, S., et al. (2012). Smchd1-dependent and -independent pathways determine developmental dynamics of CpG island methylation on the inactive X chromosome. Dev. Cell *23*, 265–279. https://doi.org/10.1016/j.devcel.2012.06.011.

Gendrel, A.V., Tang, Y.A., Suzuki, M., Godwin, J., Nesterova, T.B., Greally, J.M., Heard, E., and Brockdorff, N. (2013). Epigenetic functions of smchd1 repress gene clusters on the inactive X chromosome and on autosomes. Mol. Cell Biol. *33*, 3150–3165. https://doi.org/10.1128/mcb.00145-13.

Georgiades, P., Ogilvy, S., Duval, H., Licence, D.R., Charnock-Jones, D.S., Smith, S.K., and Print, C.G. (2002). VavCre transgenic mice: a tool for mutagenesis in hematopoietic and endothelial lineages. Genesis *34*, 251–256. https://doi.org/10.1002/gene.10161.

Goodell, M.A., and Rando, T.A. (2015). Stem cells and healthy aging. Science *350*, 1199–1204. https://doi.org/10.1126/science.aab3388.

Gordon, C.T., Xue, S., Yigit, G., Filali, H., Chen, K., Rosin, N., Yoshiura, K.I., Oufadem, M., Beck, T.J., McGowan, R., et al. (2017). De novo mutations in SMCHD1 cause Bosma arhinia microphthalmia syndrome and abrogate nasal development. Nat. Genet. *49*, 249–255. https://doi.org/10.1038/ng.3765.

Grigoryan, A., Pospiech, J., Krämer, S., Lipka, D., Liehr, T., Geiger, H., Kimura, H., Mulaw, M.A., and Florian, M.C. (2021). Attrition of X chromosome inactivation in aged hematopoietic stem cells. Stem Cell Rep. *16*, 708–716. https://doi.org/10.1016/j.stemcr.2021.03.007.

Gudmundsson, K.O., Nguyen, N., Oakley, K., Han, Y., Gudmundsdottir, B., Liu, P., Tessarollo, L., Jenkins, N.A., Copeland, N.G., and Du, Y. (2020). Prdm16 is a critical regulator of adult long-term hematopoietic stem cell quiescence. Proc. Natl. Acad. Sci. USA *117*, 31945–31953. https://doi.org/10.1073/pnas.2017626117.

Gurzau, A.D., Chen, K., Xue, S., Dai, W., Lucet, I.S., Ly, T.T.N., Reversade, B., Blewitt, M.E., and Murphy, J.M. (2018). FSHD2- and BAMS-associated mutations confer opposing effects on SMCHD1 function. J. Biol. Chem. *293*, 9841–9853. https://doi.org/10.1074/jbc.RA118.003104.

Haas, S., Trumpp, A., and Milsom, M.D. (2018). Causes and consequences of hematopoietic stem cell heterogeneity. Cell Stem Cell *22*, 627–638. https://doi.org/10.1016/j.stem.2018.04.003.

Hashimshony, T., Senderovich, N., Avital, G., Klochendler, A., de Leeuw, Y., Anavy, L., Gennert, D., Li, S., Livak, K.J., Rozenblatt-Rosen, O., et al. (2016). CEL-Seq2: sensitive highly-multiplexed single-cell RNA-Seq. Genome Biol. *17*, 77. https://doi.org/10.1186/s13059-016-0938-8.

Hope, K.J., and Sauvageau, G. (2011). Roles for MSI2 and PROX1 in hematopoietic stem cell activity. Curr. Opin. Hematol. *18*, 203–207. https://doi.org/10.1097/MOH.0b013e328347888a.

Hope, K.J., Cellot, S., Ting, S.B., MacRae, T., Mayotte, N., Iscove, N.N., and Sauvageau, G. (2010). An RNAi screen identifies Msi2 and Prox1 as having opposite roles in the regulation of hematopoietic stem cell activity. Cell Stem Cell *7*, 101–113. https://doi.org/10.1016/j.stem.2010.06.007.

Huber, W., Carey, V.J., Gentleman, R., Anders, S., Carlson, M., Carvalho, B.S., Bravo, H.C., Davis, S., Gatto, L., Girke, T., et al. (2015). Orchestrating high-throughput genomic analysis with Bioconductor. Nat. Methods *12*, 115–121. https://doi.org/10.1038/nmeth.3252.

Jansz, N., Chen, K., Murphy, J.M., and Blewitt, M.E. (2017). The epigenetic regulator SMCHD1 in development and disease. Trends Genet. *33*, 233–243. https://doi.org/10.1016/j.tig.2017.01.007.

Jansz, N., Keniry, A., Trussart, M., Bildsoe, H., Beck, T., Tonks, I.D., Mould, A.W., Hickey, P., Breslin, K., Iminitoff, M., et al. (2018). Smchd1 regulates long-range chromatin interactions on the inactive X chromosome and at Hox clusters. Nat. Struct. Mol. Biol. *25*, 766–777. https://doi.org/10.1038/s41594-018-0111-z.

Leeman, D.S., and Brunet, A. (2014). Stem cells: sex specificity in the blood. Nature *505*, 488–489. https://doi.org/10.1038/505488a.

Lemmers, R.J.L.F., van der Stoep, N., Vliet, P.J.v.d., Moore, S.A., San Leon Granado, D., Johnson, K., Topf, A., Straub, V., Evangelista, T., Mozaffar, T., et al. (2019). SMCHD1 mutation spectrum for facioscapulohumeral muscular dystrophy type 2 (FSHD2) and Bosma arhinia microphthalmia syndrome (BAMS) reveals disease-specific localisation of variants in the ATPase domain. J. Med. Genet. *56*, 693–700. https://doi.org/10.1136/jmedgenet-2019-106168.

Lemmers, R.J.L.F., Tawil, R., Petek, L.M., Balog, J., Block, G.J., Santen, G.W.E., Amell, A.M., van der Vliet, P.J., Almomani, R., Straasheijm, K.R., et al. (2012). Digenic inheritance of an SMCHD1 mutation and an FSHD-permissive D4Z4 allele causes facioscapulohumeral muscular dystrophy type 2. Nat. Genet. *44*, 1370–1374. https://doi.org/10.1038/ng.2454.

Leong, H.S., Chen, K., Hu, Y., Lee, S., Corbin, J., Pakusch, M., Murphy, J.M., Majewski, I.J., Smyth, G.K., Alexander, W.S., et al. (2013). Epigenetic regulator Smchd1 functions as a tumor suppressor. Cancer Res. *73*, 1591–1599. https://doi.org/10.1158/0008-5472.Can-12-3019.

Liao, Y., Smyth, G.K., and Shi, W. (2013). The Subread aligner: fast, accurate and scalable read mapping by seed-and-vote. Nucleic Acids Res. *41*, e108. https://doi.org/10.1093/nar/gkt214.

Liu, Y., Timani, K., Mantel, C., Fan, Y., Hangoc, G., Cooper, S., He, J.J., and Broxmeyer, H.E. (2011). TIP110/p110nrb/SART3/p110 regulation of hematopoiesis through CMYC. Blood *117*, 5643–5651. https://doi.org/10.1182/blood-2010-12-325332.

Lun, A.T.L., Chen, Y., and Smyth, G.K. (2016). It's DE-licious: a recipe for differential expression analyses of RNA-seq experiments using quasi-likelihood methods in edgeR. Methods Mol. Biol. *1418*, 391–416. https://doi.org/10.1007/978-1-4939-3578-9_19.

Mason, A.G., Slieker, R.C., Balog, J., Lemmers, R.J.L.F., Wong, C.J., Yao, Z., Lim, J.W., Filippova, G.N., Ne, E., Tawil, R., et al. (2017). SMCHD1 regulates a limited set of gene clusters on autosomal chromosomes. Skelet. Muscle *7*, 12. https://doi.org/10.1186/s13395-017-0129-7.

McCarthy, D.J., Chen, Y., and Smyth, G.K. (2012). Differential expression analysis of multifactor RNA-Seq experiments with respect to biological variation. Nucleic Acids Res. *40*, 4288–4297. https://doi.org/10.1093/nar/gks042.

Mould, A.W., Pang, Z., Pakusch, M., Tonks, I.D., Stark, M., Carrie, D., Mukhopadhyay, P., Seidel, A., Ellis, J.J., Deakin, J., et al. (2013). Smchd1 regulates a subset of autosomal genes subject to monoallelic expression in addition to being critical for X inactivation. Epigenet. Chromatin *6*, 19. https://doi.org/10.1186/1756-8935-6-19.

Nakada, D., Oguro, H., Levi, B.P., Ryan, N., Kitano, A., Saitoh, Y., Takeichi, M., Wendt, G.R., and Morrison, S.J. (2014). Oestrogen increases haematopoietic stem-cell self-renewal in females and during pregnancy. Nature *505*, 555–558. https://doi.org/10.1038/nature12932.

Ogilvy, S., Metcalf, D., Gibson, L., Bath, M.L., Harris, A.W., and Adams, J.M. (1999). Promoter elements of vav drive transgene expression *in vivo* throughout the hematopoietic compartment. Blood *94*, 1855–1863. https://doi.org/10.1182/blood.v94.6.1855.418k33_1855_1863.

Oguro, H., Ding, L., and Morrison, S. (2013). SLAM family markers resolve functionally distinct subpopulations of hematopoietic stem cells and multipotent progenitors. Cell Stem Cell *13*, 102–116. https://doi.org/10.1016/j.stem.2013.05.014.

Orkin, S.H., and Zon, L.I. (2008). Hematopoiesis: an evolving paradigm for stem cell biology. Cell *132*, 631–644. https://doi.org/10.1016/j.cell.2008.01.025.

Passegué, E., Wagers, A.J., Giuriato, S., Anderson, W.C., and Weissman, I.L. (2005). Global analysis of proliferation and cell cycle gene expression in the regulation of hematopoietic stem and progenitor cell fates. J. Exp. Med. *202*, 1599–1611. https://doi.org/10.1084/jem.20050967.

Perez-Cunningham, J., Boyer, S.W., Landon, M., and Forsberg, E.C. (2016). Hematopoietic stem cell-specific GFP-expressing transgenic mice generated by genetic excision of a pan-hematopoietic reporter gene. Exp. Hematol. *44*, 755–764.e1. https://doi.org/10.1016/j.exphem.2016.05.002.

Pietras, E., Reynaud, D., Kang, Y.A., Carlin, D., Calero-Nieto, F., Leavitt, A., Stuart, J., Göttgens, B., and Passegué, E. (2015). Functionally distinct subsets of lineage-biased multipotent progenitors control blood production in normal and regenerative conditions. Cell Stem Cell *17*, 35–46. https://doi.org/10.1016/j.stem.2015.05.003.

Risso, D., Ngai, J., Speed, T.P., and Dudoit, S. (2014). Normalization of RNA-seq data using factor analysis of control genes or samples. Nat. Biotechnol. *32*, 896–902. https://doi.org/10.1038/nbt.2931.

Ritchie, M.E., Phipson, B., Wu, D., Hu, Y., Law, C.W., Shi, W., and Smyth, G.K. (2015). Limma powers differential expression analyses for RNA-sequencing and microarray studies. Nucleic Acids Res. *43*, e47. https://doi.org/10.1093/nar/gkv007.

Rossi, D.J., Bryder, D., Zahn, J.M., Ahlenius, H., Sonu, R., Wagers, A.J., and Weissman, I.L. (2005). Cell intrinsic alterations underlie hematopoietic stem cell aging. Proc. Natl. Acad. Sci. USA *102*, 9194–9199. https://doi.org/10.1073/pnas.0503280102.

Sakakibara, Y., Nagao, K., Blewitt, M., Sasaki, H., Obuse, C., and Sado, T. (2018). Role of SmcHD1 in establishment of epigenetic states required for the maintenance of the X-inactivated state in mice. Development *145*, dev166462. https://doi.org/10.1242/dev.166462.

Shaw, N.D., Brand, H., Kupchinsky, Z.A., Bengani, H., Plummer, L., Jones, T.I., Erdin, S., Williamson, K.A., Rainger, J., Stortchevoi, A., et al. (2017). SMCHD1 mutations associated with a rare muscular dystrophy can also cause isolated arhinia and Bosma arhinia microphthalmia syndrome. Nat. Genet. *49*, 238–248. https://doi.org/10.1038/ng.3743.

Sheikh, B.N., Yang, Y., Schreuder, J., Nilsson, S.K., Bilardi, R., Carotta, S., McRae, H.M., Metcalf, D., Voss, A.K., and Thomas, T. (2016). MOZ (KAT6A) is essential for the maintenance of classically defined adult hematopoietic stem cells. Blood *128*, 2307–2318. https://doi.org/10.1182/blood-2015-10-676072.

Stadtfeld, M., and Graf, T. (2005). Assessing the role of hematopoietic plasticity for endothelial and hepatocyte development by non-invasive lineage tracing. Development *132*, 203–213. https://doi.org/10.1242/dev.01558.

Su, S., Law, C.W., Ah-Cann, C., Asselin-Labat, M.L., Blewitt, M.E., and Ritchie, M.E. (2017). Glimma: interactive graphics for gene expression analysis. Bioinformatics *33*, 2050–2052. https://doi.org/10.1093/bioinformatics/btx094.

Subramanian, A., Tamayo, P., Mootha, V.K., Mukherjee, S., Ebert, B.L., Gillette, M.A., Paulovich, A., Pomeroy, S.L., Golub, T.R., Lander, E.S., and Mesirov, J.P. (2005). Gene set enrichment analysis: a knowledge-based approach for interpreting genome-wide expression profiles. Proc. Natl. Acad. Sci. USA *102*, 15545–15550. https://doi.org/10.1073/pnas.0506580102.

Sun, D., Luo, M., Jeong, M., Rodriguez, B., Xia, Z., Hannah, R., Wang, H., Le, T., Faull, K., Chen, R., et al. (2014). Epigenomic profiling of young and aged HSCs reveals concerted changes during aging that reinforce self-renewal. Cell Stem Cell *14*, 673–688. https://doi.org/10.1016/j.stem.2014.03.002.

Syrett, C.M., Sindhava, V., Hodawadekar, S., Myles, A., Liang, G., Zhang, Y., Nandi, S., Cancro, M., Atchison, M., and Anguera, M.C. (2017). Loss of Xist RNA from the inactive X during B cell development is restored in a dynamic YY1-dependent two-step process in activated B cells. PLoS Genet. *13*, e1007050. https://doi.org/10.1371/journal.pgen.1007050.

Venezia, T.A., Merchant, A.A., Ramos, C.A., Whitehouse, N.L., Young, A.S., Shaw, C.A., and Goodell, M.A. (2004). Molecular signatures of proliferation and quiescence in hematopoietic stem cells. PLoS Biol. *2*, e301. https://doi.org/10.1371/journal.pbio.0020301.

Wang, C.Y., Colognori, D., Sunwoo, H., Wang, D., and Lee, J.T. (2019). PRC1 collaborates with SMCHD1 to fold the X-chromosome and spread Xist RNA between chromosome compartments. Nat. Commun. *10*, 2950. https://doi.org/10.1038/s41467-019-10755-3.

Wang, C.Y., Jégu, T., Chu, H.P., Oh, H.J., and Lee, J.T. (2018). SMCHD1 Merges chromosome compartments and assists formation of super-structures on the inactive X. Cell *174*, 406–421.e25. https://doi.org/10.1016/j.cell.2018.05.007.

Wang, J., Syrett, C.M., Kramer, M.C., Basu, A., Atchison, M.L., and Anguera, M.C. (2016). Unusual maintenance of X chromosome inactivation predisposes female lymphocytes for increased expression from the inactive X. Proc. Natl. Acad. Sci. USA *113*, E2029–E2038. https://doi.org/10.1073/pnas.1520113113.

Wanigasuriya, I., Gouil, Q., Kinkel, S.A., Tapia Del Fierro, A., Beck, T., Roper, E.A., Breslin, K., Stringer, J., Hutt, K., Lee, H.J., et al. (2020). Smchd1 is a maternal effect gene required for genomic imprinting. Elife *9*, e55529. https://doi.org/10.7554/eLife.55529.

Wigle, J.T., and Oliver, G. (1999). Prox1 function is required for the development of the murine lymphatic system. Cell *98*, 769–778. https://doi.org/10.1016/s0092-8674(00)81511-1.

Wigle, J.T., Harvey, N., Detmar, M., Lagutina, I., Grosveld, G., Gunn, M.D., Jackson, D.G., and Oliver, G. (2002). An essential role for Prox1 in the induction of the lymphatic endothelial cell phenotype. Embo J. *21*, 1505–1513. https://doi.org/10.1093/emboj/21.7.1505.

Wilson, A., Laurenti, E., Oser, G., van der Wath, R.C., Blanco-Bose, W., Jaworski, M., Offner, S., Dunant, C.F., Eshkind, L., Bockamp, E., et al. (2008). Hematopoietic stem cells reversibly switch from dormancy to self-renewal during homeostasis and repair. Cell *135*, 1118–1129. https://doi.org/10.1016/j.cell.2008.10.048.

Xue, Y., Liu, D., Cui, G., Ding, Y., Ai, D., Gao, S., Zhang, Y., Suo, S., Wang, X., Lv, P., et al. (2019). A 3D atlas of hematopoietic stem and progenitor cell expansion by multi-dimensional RNA-seq analysis. Cell Rep. *27*, 1567–1578.e5. https://doi.org/10.1016/j.celrep.2019.04.030.

Yildirim, E., Kirby, J., Brown, D., Mercier, F., Sadreyev, R., Scadden, D., and Lee, J. (2013). Xist RNA is a potent suppressor of hematologic cancer in mice. Cell *152*, 727–742. https://doi.org/10.1016/j.cell.2013.01.034.

Zhang, C.C., Kaba, M., Ge, G., Xie, K., Tong, W., Hug, C., and Lodish, H.F. (2006). Angiopoietin-like proteins stimulate ex vivo expansion of hematopoietic stem cells. Nat. Med. *12*, 240–245. https://doi.org/10.1038/nm1342.

Zhang, X., Jeong, M., Huang, X., Wang, X.Q., Wang, X., Zhou, W., Shamim, M.S., Gore, H., Himadewi, P., Liu, Y., et al. (2020). Large DNA methylation nadirs anchor chromatin loops maintaining hematopoietic stem cell identity. Mol. Cell *78*, 506–521.e6. https://doi.org/10.1016/j.molcel.2020.04.018.

Zheng, J., Huynh, H., Umikawa, M., Silvany, R., and Zhang, C.C. (2011). Angiopoietin-like protein 3 supports the activity of hematopoietic stem cells in the bone marrow niche. Blood *117*, 470–479. https://doi.org/10.1182/blood-2010-06-291716.

Zmuidzinas, A., Fischer, K.D., Lira, S.A., Forrester, L., Bryant, S., Bernstein, A., and Barbacid, M. (1995). The vav proto-oncogene is required early in embryogenesis but not for hematopoietic development *in vitro*. Embo J. *14*, 1–11. https://doi.org/10.1002/j.1460-2075.1995.tb06969.x.

STAR★METHODS

KEY RESOURCES TABLE

REAGENT or RESOURCE	SOURCE	IDENTIFIER
Antibodies		
Anti-mouse Flt3 (CD135) PE	BioLegend	Cat#135306; RRID: AB_1877217
Anti-mouse CD150 (TC15-12F12.2) BV421	BioLegend	Cat#115925; RRID: AB_10896787
Anti-mouse CD150 (TC15-12F12.2) PE	BioLegend	Cat#115903; RRID: AB_313682
Anti-mouse CD48 (HM48-1) FITC	BD Biosciences	Cat#557484; RRID: AB_396724
Anti-mouse CD48 (HM48-1) APC Cy7	BioLegend	Cat#103431; RRID: AB_2561462
Anti-mouse CD117 (ACK4) APC	In house	N/A
Anti-mouse Sca1 (Ly6A/E) PE Cy7	BioLegend	Cat#108114; RRID: AB_493596
Anti-mouse Sca1 (Ly6A/E) PE Cy7	BD Biosciences	Cat#558162; RRID: AB_647253
Anti-mouse CD45.1 (A20) FITC	BioLegend	Cat#110706; RRID: AB_313495
Anti-mouse CD45.2 (S450-15-2) FITC	In house	N/A
Anti-mouse CD45.2 (S450-15-2) PE	In house	N/A
Anti-mouse CD45.2 (104) PE	BioLegend	Cat#109807; RRID: AB_313444
Anti-mouse CD45.2 (104) Alexa700	BioLegend	Cat#109822; RRID: AB_493731
Anti-mouse CD4 (GK1.5) PE	In house	N/A
Anti-mouse CD4 (GK1.5) APC	In house	N/A
Anti-mouse CD4 (GK1.5) Alexa700	In house	N/A
Anti-mouse CD8a (53-6.7) unconjugated	In house	N/A
Anti-mouse CD8a (53-6.7) PE	In house	N/A
Anti-mouse CD8a (53-6.7) Alexa700	In house	N/A
Anti-mouse B220 (RA3-6B2) unconjugated	In house	N/A
Anti-mouse B220 (RA3-6B2) APC	In house	N/A
Anti-mouse B220 (RA3-6B2) Alexa700	In house	N/A
Anti-mouse B220 (RA3-6B2) APC Cy7	BD Biosciences	Cat#552094; RRID: AB_394335
Anti-mouse CD19 (1D3) unconjugated	In house	N/A
Anti-mouse CD19 (1D3) PE Cy7	BD Biosciences	Cat#552854; RRID: AB_394495
Anti-mouse CD25 (PC61.6) PE Cy7	eBiosciences	Cat#25-0251-82;RRID: AB_469608
Anti-mouse IgM (5.1) PE	In house	N/A
Anti-mouse Ter119 (TER-119) unconjugated	In house	N/A
Anti-mouse Ter119 (TER-119) Alexa700	In house	N/A
Anti-mouse Gr1 (RB6-8C5) unconjugated	In house	N/A
Anti-mouse Gr1 (RB6-8C5) PE	In house	N/A
Anti-mouse Gr1 (RB6-8C5) Alexa700	In house	N/A
Anti-mouse Mac1 (M1/70) unconjugated	In house	N/A
Anti-mouse Mac1 (M1/70) APC	In house	N/A
Anti-mouse Mac1 (M1/70) Alexa700	In house	N/A
Anti-mouse Ly6G (1A8) Alexa700	In house	N/A
Anti-mouse CD3 (KT3.1.1) unconjugated	In house	N/A
Anti-mouse CD3 (KT3.1.1) Alexa700	In house	N/A
Anti-mouse CD2 (Rm2.1) unconjugated	In house	N/A

(*Continued on next page*)

Continued

REAGENT or RESOURCE	SOURCE	IDENTIFIER
Critical commercial assays		
Cytofix/Cytoperm Fixation Permeabilization Solution	BD Biosciences	Cat#554714
Mouse Ki67 antibody/isotype control set (FITC)	BD Biosciences	Cat#556026
Deposited data		
Minibulk RNA-Seq on Smchd1-del HSCs	This study	GEO: GSE188517
RNA-Seq on Smchd1-del B cells	This study	GEO: GSE188685
SuperSeries record	This study	GEO: GSE188686
Experimental models: Organisms/strains		
Smchd1$^{GFP/GFP}$ mouse strain	Jansz et al., 2018	N/A
Smchd1-Vav.Cre mouse strain	This study	N/A
Oligonucleotides		
Oligonucleotides for genotyping are given in Table S1	Jansz et al., 2018 de Greef et al., 2018	N/A
Software and algorithms		
Subread aligner	PMID: 23558742	v2.4.2
R	R Core Team (https://www.R-project.org/)	v4.0.3
Bioconductor	PMID: 25633503	v3.12
edgeR	PMID: 27508061	v3.32.1
Glimma	PMID: 28203714	v2.0.0
Limma	PMID: 25605792	v3.36.0
FastQC	http://www.bioinformatics.babraham.ac.uk/projects/fastqc	v0.11.5
Trim_galore!	http://www.bioinformatics.babraham.ac.uk/projects/trim_galore/	RRID:SCR_011847 v0.4.1
TopHat	PMID:23618408; PMID:19289445	RRID:SCR_013035 v2.1.1
Seqmonk	https://www.bioinformatics.babraham.ac.uk/projects/seqmonk/	v1.48.0
Other		
Analysis code	This study	https://doi.org/10.5281/zenodo.6680651

RESOURCE AVAILABILITY

Lead contact

Any further information and requests for resources and reagents should be directed to and will be fulfilled by the lead contact, Marnie Blewitt (blewitt@wehi.edu.au).

Material availability

All biological materials are available upon request to the lead contact.

Data and code availability

Raw data are available under GEO: GSE188517 for the Smchd1-del LT-HSC RNA-Seq and GEO: GSE188685 for the Smchd1-del B cell RNA-Seq, with the SuperSeries Record available at GEO: GSE188686. All processed data and scripts are available from Github (https://github.com/WEHISCORE/C086_Kinkel). Any other information required for data analysis or to access any other data, please contact the lead author.

EXPERIMENTAL MODEL AND SUBJECT DETAILS

Animal husbandry and ethics

All mice were bred and maintained under specific pathogen-free conditions at The Walter and Eliza Hall Institute where they were housed in groups of a maximum of six mice per cage and were kept on a 14h

day and 10h night cycle, at a temperature of 20–22°C with 30–45% humidity levels. All experiments were performed at The Walter and Eliza Hall Institute and approved by the local Animal Ethics Committee (AEC 2014.034, 2018.004, 2020.048 and 2020.050).

Smchd1$^{GFP/GFP}$ mice

The *Smchd1*^{GFP} allele was backcrossed to C57BL/6 for more than 10 generations and kept as a homozygous breeding line (Jansz et al., 2018). Mice used for Smchd1-GFP expression by flow cytometry were grouped into young (4- to 7-months old) or aged (12- to 18-months old) animals and were separated by sex.

Smchd1- Vav.Cre mice

To generate mice with a blood lineage-specific deletion of *Smchd1* on a C57BL/6 strain background, female *Smchd1*$^{fl/fl}$ animals (de Greef et al., 2018) were crossed to males heterozygous for a deleted allele of *Smchd1* derived from the *Smchd1*^{fl} allele (*Smchd1*$^{del/+}$) that also carried a *Vav.Cre* transgene (*Vav.Cre*$^{T/+}$) (Croker et al., 2004). As the *Vav.Cre* transgene has been shown to be expressed and cause recombination in the germline (Croker et al., 2004; Ogilvy et al.,1999), our breeding strategy was designed to prevent germline deletion of *Smchd1* by ensuring that *Vav.Cre*$^{T/+}$ breeders also carry a *Smchd1*$^{+}$ allele that cannot be deleted. This breeding strategy means that we do not produce any *Smchd1*$^{+/+}$ *Vav.Cre*$^{T/+}$ animals. Our previous studies have shown no major differences in the hematopoietic phenotype between wild-type and *Smchd1* heterozygous mice (Leong et al., 2013) and data from our current study demonstrates comparable blood cell numbers and proportions between *Smchd1*$^{fl/+}$ *Vav.Cre*$^{T/+}$ mice and wild-type animals of the same C57BL/6 genetic background [Jackson Laboratory: Physiological Data Summary – Aged C57BL/6J (000664)]. We therefore used *Smchd1*$^{fl/+}$ *Vav.Cre*$^{T/+}$ mice as controls, allowing us to maximize the proportion of usable offspring produced from our breeding crosses, which is an important animal ethics consideration. Mice were grouped into young (4- to 8-months old) or aged (12- to 18-months old) animals, with male and female mice analyzed separately and the sex of animals noted in the results. For the HSC RNAseq, LT-HSCs were sorted from 2- to 5-months old female mice. For the B cell RNAseq, B cells were sorted from 12- to 16-months old male and female mice and analyzed as separate groups dependent on sex and genotype.

Smchd1^{MommeD1} mice

Mice carrying the *Smchd1*^{MommeD1} mutant allele were maintained on the FVB/N inbred background (Blewitt et al., 2008; Jansz et al., 2018). Mice analyzed for peripheral blood cell counts were 6- to 12-weeks of age and only male mice were used.

METHOD DETAILS

Genotyping

Ear clip samples taken from mice at weaning were digested using DirectPCR Lysis Buffer (Viagen) with 0.4 mg/mL Proteinase K (Sigma) at 55°C for a minimum of 2 h, followed by Proteinase K inactivation at 85°C for 45 min. Lysates were used directly for genotyping by PCR using GoTaq Green (Promega) with specific-primers (Table S1) and the following cycle conditions: 94°C for 5 min, 30 cycles of 94°C for 30 s, 60°C for 30 s and 72°C for 1 min, followed by a final incubation at 72°C for 7 min. The *Smchd1*$^{GFP/GFP}$ strain was genotyped by PCR using oligos specific to the integration site. For the *Smchd1-Vav.Cre* mice, multiplexed genotyping primers were used to differentiate between the wild type, *Smchd1*^{fl} conditional and *Smchd1*^{del} alleles, while the *Vav.Cre* transgene was genotyped using a general Cre PCR (Table S1). For the *Smchd1-Vav.Cre* strain, deletion of the *Smchd1*^{fl} conditional allele was confirmed in thymus, spleen and/or bone marrow-derived hematopoietic cells collected from animals at the time of sacrifice. Genotyping of the *Smchd1*^{MommeD1} strain was performed a by allelic discrimination using a custom Taqman assay designed to detect the mutant and wild-type alleles (Table S1). Reactions of 10μL volume with DNA, dH2O, 40x SNP Taqman mix containing allelic discrimination probes (Applied Biosystems) and 2x Taqman Universal Master Mix with no AmpErase UNG (Applied Biosystems) were prepared in MicroAmp Optical 384-well reaction plates (Applied Biosystems) in duplicate per sample. Samples were run on the QuantStudio 12K Real-Time PCR System (Thermo Fisher) using the following PCR cycle conditions: 50°C for 2 min, 95°C for 10 min, 40 cycles of 92°C for 15 s, and 60°C for 1 min. Genotypes were determined using the QuantStudio 12K Flex software v1.5 (Thermo Fisher).

Peripheral blood analysis

Peripheral blood was collected from mice via the retro-orbital sinus into EDTA-coated tubes (Sarstedt). Automated blood counts were performed using the ADVIA 2120i Hematology System (Bayer) on whole blood or blood diluted 1:2 with PBS. For flow cytometric analysis, whole blood was treated with red cell removal buffer (NH_4Cl: generated in house), then washed and resuspended FACS buffer (generated in house: PBS with 5% FCS (Hyclone) and 2mM EDTA).

Hematopoietic organ analysis by flow cytometry

Single cell suspensions from thymus and spleen were generated by mashing cells through a 100μm cell-strainer (Falcon) with the plunger from a 3mL plastic syringe (Termuno). Cells were then treated briefly with red cell removal buffer (NH_4Cl: generated in house), then washed and resuspended in FACS buffer (generated in house: PBS with 5% FCS (Hyclone) and 2mM EDTA). Bone marrow was collected from the iliac, tibia and femur bones by flushing with sterile FACS buffer (generated in house: PBS with 5% FCS (Hyclone) and 2mM EDTA) using a 22G BD Precision Glide Needle (Sigma-Aldrich) attached to a 1mL or 3mL syringe (Terumo). Cells were then passed through a 100μm cell-strainer (Falcon) to removed bone fragments and treated with red cell removal buffer (NH_4Cl: generated in house) before being washed and resuspended in FACS buffer (generated in house: PBS with 5% FCS (Hyclone) and 2mM EDTA). For lineage depletion, bone marrow cells were then stained with rat monoclonal antibodies against lineage markers (Ter119, B220, CD19, Mac1, Gr1, CD2, CD3, CD8 all from the Walter & Eliza Hall Institute Monoclonal Antibody Facility) and then incubated with BioMag goat anti-rat IgG beads (Qiagen) for magnetic depletion. Cells were stained with fluorochrome conjugated antibodies in FACS buffer to identify the cell types specified for a minimum of 30 min at 4°C. Cell surface markers used to identify different cell types are indicated in the figures or text. Cells were stained with FluoroGold (Santa-Cruz Biotechnology) or 7-AAD (Thermo-Fisher Scientific) for identification and exclusion of dead cells. Cell numbers were quantified by adding known numbers of counting beads (BD Biosciences) that were gated based on low forward scatter and high side scatter by flow cytometry, with numbers of beads collected compared to the number added used to estimate total cell numbers. Flow cytometry was performed on the Fortessa X20 (BD Biosciences; FACSDiva Software) and data analyzed using FlowJo 10 (Treestar).

Cell cycle analysis

Bone marrow from femurs and tibias was depleted for red blood cells and cells expressing mature lineage markers as described above. Lineage-depleted BM was then stained for LT-HSCs using the following antibodies: Alexa-700 conjugated lineage antibodies (Ter119, B220, Mac1, Gr1, Ly6G and CD3), c-kit-APC, Sca1-PECy7, CD48-APCCy7 and CD150-PE, in FACS buffer (generated in house: PBS with 5% FCS (Hyclone) and 2mM EDTA) for 40′ on ice. Cells were washed with FACS buffer and then fixed in 500μL BD Cytofix/Cytoperm buffer (BD Biosciences) for 45 min on ice. Fixed cells were washed twice with 4mL 1x BD Perm/Wash buffer (BD Biosciences) by centrifugation for 5′ at 220 x g at 4°C and then stained with 20μL FITC-conjugated mouse anti-Ki67 antibody or isotype control (BD Biosciences) in the dark for 18 h at 4°C. Cells were washed twice with 1x BD Perm/Wash buffer (BD Biosciences), incubated with 10 μg/mL DAPI in 1x BD Perm/Wash buffer for 30′ on ice and then washed with and resuspended in FACS buffer for flow cytometry. Ki67 staining and DNA content was analyzed on the BD Symphony (BD Biosciences) and using FlowJo 10 software (TreeStar).

Competitive bone marrow transplantation assays

For 10:1 competitive bone marrow transplantation assays, bone marrow was collected from the tibia and femur bones by flushing with sterile FACS buffer (generated in house: PBS with 5% FCS (Hyclone) and 2mM EDTA) using a 22G BD Precision Glide Needle (Sigma-Aldrich) attached to a 1mL or 3mL syringe (Terumo). Cells were passed through a 100μm cell-strainer (Falcon) to removed bone fragments and washed a minimum of three times with sterile FACS buffer. An aliquot of each sample was then diluted, stained with trypan blue (0.4%, Gibco) and counted on a hemocytometer (Marienfeld) to determine cell concentration. 2×10^6 $CD45.2^+$ control (*Smchd1*$^{fl/+}$ *Vav.Cre*$^{T/+}$) or Smchd1-del (*Smchd1*$^{del/fl}$ *Vav.Cre*$^{T/+}$) bone marrow cells were mixed with 2×10^5 *Smchd1*$^{+/+}$ bone marrow cells from young $CD45.1^+/CD45.2^+$ female mice. Mixed whole bone marrow cells were injected *i.v.* in 200μL saline buffer into the tail vein of lethally irradiated (2 × 5.5Gy doses) female $CD45.1^+$ recipients with two recipient animals per donor. An aliquot of each test/competitor bone marrow cell mix was stained

with antibodies to differentiate CD45.2$^+$ cells from CD45.1$^+$/CD45.2$^+$ cells and analyzed by flow cytometry to confirm the 10:1 input ratio.

For secondary bone marrow transplants, whole bone marrow cells from primary transplant recipients were collected and treated as described above. 5 × 10^6 bone marrow cells were injected into two lethally irradiated (2 × 5.5Gy doses) female CD45.1$^+$ secondary recipients per donor.

For homing assays, 10 × 10^6 CD45.2$^+$ control (*Smchd1$^{fl/+}$ Vav.Cre$^{T/+}$*) or Smchd1-del (*Smchd1$^{del/fl}$ Vav.Cre$^{T/+}$*) bone marrow cells were mixed with 1 × 10^6 *Smchd1$^{+/+}$* bone marrow cells from young CD45.1$^+$/CD45.2$^+$ female mice. Mixed whole bone marrow cells were injected *i.v.* in 200μL saline buffer into the tail vein of lethally irradiated (2 × 5.5Gy doses) female CD45.1$^+$ recipients with four recipient animals per donor. An aliquot of each test/competitor bone marrow cell mix was stained with antibodies to identify HSPCs and differentiate CD45.2$^+$ cells from CD45.1$^+$/CD45.2$^+$ cells, these cells were analyzed by flow cytometry to confirm the 10:1 input ratio. Recipients were analyzed at 18 h post-transplantation to determine the homing capacity of test donor cells. Recipient bone marrow was RCRB-treated and stained for mature cell lineage markers, c-kit and Sca1, as well as CD45.1 and CD45.2 to discriminate between test, competitor and recipient cells. The proportion of test cells within the donor lineage$^-$ BM population (output) was compared to the proportion within the transplanted HSPC/LSK population (input).

For sorted LT-HSC competitive transplantation assays, bone marrow was collected from the iliac, tibia and femur bones by flushing with sterile FACS buffer using a 22G BD Precision Glide Needle (Sigma-Aldrich) attached to a 1mL or 3mL syringe (Terumo). Cells were passed through a 100μm cell-strainer to removed bone fragments and washed a minimum of three times with sterile FACS buffer. Cells were depleted for lineage positive cells as described above and then stained with antibodies. 200 LT-HSCs (Ter119$^-$ B220$^-$ Mac1$^-$ Gr1$^-$ Ly6G$^-$ CD3$^-$ c-kit$^+$ Sca1$^+$ Flt3$^-$ CD48$^-$ CD150$^+$) were sorted from test donors using the FACSAria (BD Biosciences; FACSDiva Software) and mixed with 4 × 10^5 whole bone marrow cells from young, sex-matched CD45.1$^+$/CD45.2$^+$ mice for injection into lethally irradiated (2 × 5.5Gy doses) sex-matched CD45.1$^+$ recipients, with 2 or 3 recipients per donor. All transplant recipients were maintained on antibiotic supplemented drinking water (neomycin (Sigma-Aldrich) 1.1g/L) for three weeks post-irradiation. Peripheral blood and relevant organs were collected for analysis at the times post-transplant as indicated.

HSC minibulk RNA-Seq

Cell sort

Triplicate wells of 100 lineage$^-$ (Ter119$^-$ Gr1$^-$ Mac1$^-$ CD3$^-$ Ly6G$^-$ B220$^-$) c-kit$^+$ Sca1$^+$ Flt3$^-$ CD48$^-$ CD150$^+$ LT-HSCs were sorted per individual animal on the Aria Fusion (BD Biosciences) from 3 control males, 3 control females, 2 Smchd1-del males and 1 Smchd1-del female; for a further 2 Smchd1-del females wells containing 100, 100, 58 and 100, 50 LT-HSCs were sorted. Mice were littermates or age-matched cage-mate controls aged between 80 and 180 days old. LT-HSCs were flow sorted into a chilled 384-well PCR plate (Greiner, 785290), with each well containing 1.2μL of primer/lysis mix [20 nM indexed polydT primer (custom made, IDT), 1:6.000.000 dilution of ERCC RNA spike-in mix (Ambion - 4456740), 1 mM dNTPs (NEB, N0446S), 1.2 units SUPERaseIN Rnase Inhibitor (Thermo Fisher - AM2696), 0.2% Triton X-100 solution (Sigma Aldrich, 93443–100mL), DEPC water (Thermo Fisher, AM9920)] using a BD FACSAria III flow cytometer (BD Biosciences). Sorted plates were sealed, centrifuged for 1 min at 3000 rpm and immediately frozen upside down at −80C until further processing using an adapted CelSeq2 protocol (Hashimshony et al., 2016).

cDNA generation and pooling

Sorted plates were thawed on ice and briefly centrifuged. To lyse the cells and anneal the mRNA capture primer the plate was incubated at 65°C for 5 min and immediately chilled on ice for at least 2 min before adding 0.8μL reverse transcription reaction mix [in 2μL RT reaction: 1x First Strand buffer (Invitrogen, 18064-014), 20 mM DTT (Invitrogen, 18064-014), 4U RNaseOUT (Invitrogen, 10777-019), 10U SuperScript II (Invitrogen, 18064-014)]. The plate was incubated at 42°C for 1 h, 70°C for 10 min and chilled to 4°C to generate first strand cDNA. Samples were pooled by placing the plate upside down on a trough (Nalgene, VP 792D) using a home-made 3D printed adapter to hold plate in place. The combined plate/trough stack was place in a plate centrifuge and spun at 1,500 rpm for 1 min. Using a P1000 pipette the sample was transferred into a fresh 1.5 mL Eppendorf LoBind tube (Eppendorf, 0030108051).

Exonuclease treatment and clean-up

Exo I (NEB - M0293L; 20 U/ul) was added to the pooled sample at a final concentration 1 U/ul concentration and gently mixed by pipetting. In a heat block the sample was incubated at 37C for 30 min, followed by 80°C for 10 min and placed on ice. Once samples reached room temperature a 1.2X NucleoMag NGS Clean-up and Size select magnetic beads (Macherey-Nagel, 7449970.5) clean-up was performed according to manufactures instruction. To reduce the number of beads for each 100µL pooled sample 20µL beads and 100µL bead binding buffer (20% PEG8000, 2.5M NaCl, pH5.5) was added. The cDNA was eluted in 17 µL DEPC water and transferred to a fresh 0.2 mL PCR tube.

Second strand DNA synthesis

3µL of second strand reaction mix was added to the sample [1x NEBNext Second Strand Synthesis buffer (NEB #E6111S), NEBNext Second Strand Synthesis Enzyme Mix: 2.4U DNA Polymerase I (*E. coli*), 2U RNase H, 10U *E. coli* DNA Ligase (NEB #E6111S), DEPC water (Thermo Fisher, AM9920)]. The sample was gently mixed by pipetting and incubated at 16°C for 2 h in a thermal cycle with unheated lid to generate double stranded cDNA followed by a 1.2X NucleoMag NGS Clean-up and Size select magnetic beads (Macherey-Nagel, 7449970.5) clean-up according to manufactures instruction. The cDNA was eluted in 6.4 µL DEPC water and kept with beads for the following IVT reaction.

In vitro transcription

9.6µL of IVT reaction mix [1.6µL of each of the following: ATP, GTP, CTP, UTP solution, 10X T7 buffer, T7 enzyme (MEGAscript T7 Transcription Kit, Ambion, AM1334) was added and incubated at 37°C for 13 h and then chilled and kept at 4°C. To remove leftover primers 6µL ExoSAP-IT. For PCR Product Clean-Up (Affymetrix, 78200) was added and the sample was incubated at 37°C for 15 min, then chilled and kept at 4°C.

RNA fragmentation and clean-up

Chemical heat fragmentation was performed by adding 5.5µL of 10X Fragmentation buffer (Thermo Fisher, AM8740) to the sample and incubation in pre-heated thermal cycler at 94°C for 2.5 min followed by immediately chill on ice and addition of 2.75µL of Fragmentation Stop buffer (Thermo Fisher, AM8740). The fragmented amplified RNA was purified using 1.8X RNAClean XP beads (Beckman coulter, A63987) according to manufactures instruction and eluted in 6µL DEPC water of which 5µL (no beads) were transferred to a fresh tube for library preparation.

5'-tagged-random-hexamer reverse transcription

The fragmented RNA was transcribed into cDNA using 5'-tagged random hexamer primers 9 (GCCTTGGCACCCGAGAATTCCANNNNNN) introducing a partial Illumina adapter as also described in CEL-Seq2 [Hashimshony, 2016 #73]. To remove RNA secondary structure and anneal the mRNA capture primer 1µL of tagged random hexamer (100µM) and 0.5µL of 10mM dNTPs (dNTP solution set; NEB, N0446S) were added to the sample and incubated at 65°C for 5 min and immediately chilled on ice for at least 2 min before adding 4µL reverse transcription reaction mix (in 10µL RT reaction: 1x Fist Strand buffer (Invitrogen, 18064-014), 20 mM DTT (Invitrogen, 18064-014), 4U RNaseOUT (Invitrogen, 10777-019), 10U SuperScript II (Invitrogen, 18064-014)).

Library amplification and cleanup

The PCR primers introduce the full-length adaptor sequence required for Illumina sequencing (for details see Illumina small RNA PCR primers). PCR was performed in 12.5µL using half of the ranhexRT sample as a template (1X KAPA HiFi HotStart ReadyMix (KapaBiosystems KK2602), 400 nM each primer). The final PCR amplified Library was submitted to two consecutive 1x NucleoMag NGS Clean-up and Size select magnetic beads (Macherey-Nagel, 7449970.5) according to manufacturer's instruction. The final library was eluted in 20µL of 10 mM Trizma hydrochlorid solution (Sigma-Aldrich, T2319-1L).

NextSeq sequencing

The pooled (MiniBulk) low input indexed libraries were diluted to 1.5p.m. for paired end sequencing (1 × 15/1 × 71 cycles plus 6 base index cycle) on a NextSeq 500 instrument using the v2 75 cycle High Output kit (Illumina) as per manufacturer's instructions. The base calling and quality scoring were determined using Real-Time Analysis on board software v2.11.3, while the FASTQ file generation and de-multiplexing utilized bcl2fastq conversion software v2.15.0.4.

HSC minibulk RNA-Seq analysis

Mini-bulk reads were mapped to the GRCm38.p6 mouse reference genome and ERCC spike-in sequences using the Subread aligner (v2.4.2) (Liao et al., 2013) and assigned to genes using scPipe (v1.12.0) with GENCODE M18 primary assembly annotation. Gene counts were exported as a matrix by scPipe as read counts (i.e. ignoring UMI sequences). All subsequent analyses were performed in R (v4.0.3) (R Foundation for Statistical Computing, Vienna, Austria, 2021) with Bioconductor (v3.12) (Huber et al., 2015).

We then focused on samples from the female mice and aggregated the technical replicates by summing the read counts, resulting in n = 3 (Del) and n = 3 (Het) biological replicates for each of the genotypes.

We filtered the genes to only retain those annotated as protein coding and then applied the 'filterByExpr' function in edgeR (v3.32.1) (Chen et al., 2016) to determine which genes had sufficiently large counts to be retained in a differential expression analysis (11,513 genes). We then normalized the filtered counts using upper-quartile (UQ) normalization (Bullard et al., 2010).

Upon visualizing the data using multidimensional scaling (MDS) of the log-counts-per-million (logCPM), we decided that further normalization was required. We applied RUVs, as implemented in RUVSeq (v1.24.0) (Risso et al., 2014), to estimate the factors of unwanted variation using replicate/negative control samples for which the covariates of interest are constant. Specifically, we treated samples with the same genotype as replicate groups, used all genes to estimate the unwanted variation (shown to work well in practice by Risso et al.) (Risso et al., 2014), and estimated k = 1 factor of unwanted variation (W).

Our primary comparison of interest was to identify differentially expressed genes (DEGs) between the Del and Het groups. To do so, we used the likelihood ratio testing framework implemented in the edgeR package (v3.32.1) (McCarthy et al., 2012) with an additive design matrix that included a term for the group and the unwanted variation (W). The results of the DE analysis were interactively explored using Glimma (v2.0.0) (Su et al., 2017) and visualized as heatmaps using the pheatmap package (v1.0.12). The DEG list is available in Table S2.

Mini-bulk RNA-seq data are available through the Gene Expression Omnibus under accession number GSE188517. All scripts used in the processing and analysis of the mini-bulk RNA-seq data are available from https://github.com/WEHISCORE/C086_Kinkel.

B cell bulk RNA-Seq

CD45.2^{+} B220^{+} Mac1^{-} B cells were sorted from the bone marrow of 5 female and 4 male Smchd1-del animals at 12–16 months of age alongside matched littermate heterozygous controls. Cells were sorted using the FACSAria (BD Biosciences; FACSDiva Software). RNA and DNA were extracted using a Zymo Quick DNA/RNA miniprep plus kit as per manufacturer's instructions. Deletion of *Smchd1* was confirmed by genotyping PCR described above. Sequencing libraries were prepared using the TruSeq RNA Sample Preparation Kit (Illumina). Fragments were size selected using AMPure XP magnetic beads (Beckman Coulter). Libraries were quantified with a D1000 tape on a 4,200 Tapestation (Agilent), then pooled and sequenced in house on the Illumina NextSeq platform with 75bp single end reads for the female samples and paired end reads for the males. Base calling was done using Real-Time Analysis v2.4.6, demultiplexing and fastq.gz file generation was done using bcl2fastq.

Quality control and adapter trimming were performed with FastQC and Trim_galore! and reads were aligned to the mm10 reference genome annotation using TopHat. Expression values in reads per million were determined using the the RNA-seq Quantitation Pipeline from Seqmonk (www.bioinformatics.babraham.ac.uk/projects/seqmonk/), selecting the merged transcripts counting reads over exons as raw counts option to generate the raw count matrices. We applied the 'filterByExpr' function in edgeR (v3.32.1) (Chen et al., 2016) to determine which genes had sufficiently large counts to be retained in a differential expression analysis (13,498 genes). We then normalized the filtered counts using upper-quartile (UQ) normalization (Bullard et al., 2010).

Our primary comparison of interest was to identify differentially expressed genes (DEGs) between the Del and Het groups. To do so, we used the quasi-likelihood framework implemented in the edgeR package (v3.32.1) (Lun et al., 2016) with an additive design matrix that included a term for the group. The results

of the DE analysis were interactively explored using Glimma (v2.0.0) (Su et al., 2017) and visualized as heatmaps using the pheatmap package (v1.0.12). The DEG lists are available in Tables S3 and S4.

RNA-seq data are available through the Gene Expression Omnibus under accession number GSE188685. All scripts used in the analysis of the B cell RNA-seq data are available from https://github.com/WEHISCORE/C086_Kinkel.

Gene set testing

We tested for over representation of gene ontology terms and KEGG pathways in the resulting gene lists using the 'goana' and 'kegga' functions from limma (v3.46.0) (Ritchie et al., 2015). We applied the 'camera' function from limma (v3.46.0) to test the Hallmark and C2 gene sets from MSigDB (Subramanian et al., 2005) for whether these were highly ranked relative to other genes in terms of differential expression. We used the 'fry' function to test if genes in various other gene sets, as described in the results section, were differentially expressed. We visualized the expression of specific gene sets using barcode plots.

RT-qPCR

RNA was extracted from sorted Lin^- $ckit^+$ cells using Quick-RNA Miniprep Kit (Zymo) with an on-column DNase digest, or from B cells as described above. cDNA was generated using 200U SuperScript III RT (Life Technologies) with $oligo(dT)_{15}$ (Promega) priming, as per manufacturer's instructions. Real time PCR was performed on the LightCycler LC480 Real-Time PCR instrument (Roche) using TaqMan Universal PCR Master Mix (Applied Biosystems) and gene specific TaqMan assays (Applied Biosystems) for *Hprt* (Mm01545399), *Hmbs* (Mm01545399), *Smchd1* (Mm00512253) and *Prox1* (Mm00435969) with manufacturer recommended cycling conditions. Cycle threshold (Ct) values were determined using the LightCycler 480 software. Relative mRNA expression levels were calculated by the 2^{-ddCt} method after first normalizing to the geometric mean of the Ct values of housekeeping genes *Hprt* and *Hmbs* and then comparing to one of the sex matched controls.

QUANTIFICATION AND STATISTICAL ANALYSIS

All information pertaining to statistical tests and significance can be found in the figure legends. For peripheral blood and organ analysis of unmanipulated mice or bone marrow recipients, the number of animals analyzed is indicated by the number of individual points represented each graph, with columns representing mean and error bars SEM. These data were statistically analyzed by one-way ANOVA with Sidak multiple comparisons test comparing control and Smchd1-del for each sex using Prism 9. Analysis of peripheral blood and hematopoietic organs of young and aged mice was performed over multiple experimental days but always with sex and age-matched control/test pairs. Competitive bone marrow transplantation experiments were repeated at least twice, except for the female sorted HSCs transplantation, which was performed once. Outliers were not removed, but transplant recipient animals that developed radiation-induced $CD45.1^+$ recipient cell-derived thymoma as confirmed by flow cytometry were removed from the analysis.